PHYSICAL REVIEW B VOLUME 28, NUMBER 10 15 NOVEMBER 1983

Order, frustration, and defects in liquids and glasses

David R. Nelson
Lyman Laboratory of Physics, Harvard University, Cambridge, Massachusetts 02138
(Received 19 May 1983)

A defect description of liquids and metallic glasses is developed. In two dimensions, surfaces of constant negative curvature contain an irreducible density of point disclinations in a hexatic order parameter. Analogous defect lines in an icosahedral order parameter appear in three-dimensional flat space. Frustration in tetrahedral particle packings forces disclination lines into the medium in a way reminiscent of Abrikosov flux lines in a type-II superconductor and of uniformly frustrated spin-glasses. The defect density is determined by an isotropic curvature mismatch, and the resulting singular lines run in all directions. The Frank-Kasper phases of transition-metal alloys are ordered networks of these lines, which, when disordered, provide an appealing model for structure in metallic glasses.

I. INTRODUCTION

Structure in dense liquids and metallic glasses is intimately connected with the difficulty in close-packing space with tetrahedra.[1] In simple materials, without directional bonding, one minimizes the local-energy density by forming tetrahedral clusters of four identical particles. The *frustration* associated with tetrahedral packings becomes apparent, however, when twenty tetrahedra combine to form a 13-atom icosahedron. As shown in Fig. 1(a) the twelve particles symmetrically arranged about a central one are not packed perfectly, because the distance between these surface atoms is about 5% larger than the distance to the center. If one tries to move the surface atoms closer together, still keeping them a constant distance from the central sphere, the cracks between surface particles in the symmetrical arrangement coalesce into a larger open space somewhere on the surface. This excess "free volume" (which is not large enough to accommodate a thirteenth surface atom) is an important source of degeneracy and frustration in dense-random-packing models of the glassy state. The surface atoms are "frustrated," because atoms near the gap cannot simultaneously sit at the minima of pairwise interactions with all their near neighbors.

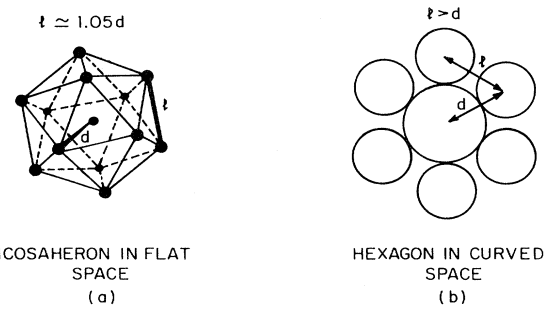

FIG. 1. Comparison of the icosahedron in flat space and a hexagon projected out of a space of constant negative curvature. Apparent size difference in the disks comprising the hexagon is an artifact of the projection. In both cases, the distance l between the centers of the particles on the surface is larger than the distance d to the center.

Icosahedra should also be prevalent in liquids near the melting temperature. As pointed out by Frank,[2] icosahedral clusters of 13 particles have a significantly lower energy than more obvious "crystallographic" arrangements, corresponding to nuclei of fcc and hcp crystals.[3] Frank appealed to an abundance of icosahedral clusters to explain the remarkable degree of supercooling possible in simple liquid metals.[4] Recently, Steinhardt *et al.* have studied bond orientational order in a computer simulation of supercooled Lennard-Jones liquids.[5] Icosahedra dominate at sufficiently low temperatures with correlations that become comparable to the 864-atom system size upon supercooling about 10% below the equilibrium melting temperature. Extended icosahedral correlations were also found in small "amorphon" cluster models of structure in metallic glasses.[6]

To make theoretical progress it is clearly desirable to parametrize frustration in icosahedra in such a way that it can be tuned to zero. An important observation was made by Coxeter,[7–9] who showed how tetrahedra could be packed without frustration on the surface $S3$ of a four-dimensional (4D) sphere. All 120 particles in this finite tesselation have icosahedral coordination shells, with no gaps between the surface atoms. Clearly, curvature can be used to vary the frustration. This idea has been developed recently by Kléman and Sadoc, who view dense random packing as a mapping into flat space of tetrahedra which tile a space with an appropriately chosen curvature.[10] Mappings from spaces of negative[11] and positive[12] curvatures have been proposed, leading to various kinds of defects, including disclinations. Unfortunately, the ideal tesselation in hyperbolic space is pathological because every particle has an infinite number of nearest neighbors (see below). When the physically more sensible embedding of the finite space $S3$ is used, the mapping introduces not only disclinations, but also ambiguous regions of overlap between squashed 4D spheres.[13]

In this paper, we use the idea of an ideal $S3$ tessellation

in a slightly different way: Supercooled liquids and metallic glasses are viewed as defected states of icosahedral bond orientational order. At higher temperatures a variety of disclination lines [each characterized by an SU(2) matrix charge] are present, and the incompatibility of flat space with tiling tetrahedra is hardly noticeable. As one cools the melt, defect lines with opposite charges pair gradually until an excess of one particular species becomes evident. This excess is associated with the curvature difference between the "ideal" space $S3$ and ordinary three-dimensional (3D) flat space. At low temperatures the defects form networks much like the Abrikosov flux lines in type-II superconductors. Because an *isotropic* curvature mismatch plays the role of an applied magnetic field, the lines run in all directions. The "Frank-Kasper" phases of complex alloy systems[14] are in fact ordered arrays of these lines with a spacing determined by the curvature "incommensurability." Upon disordering a Frank-Kasper disclination network, one obtains an attractive model for a metallic glass. Although we refer to the ideal curved-space tessellation of $S3$ to determine an excess defect density, the cooling process is to be carried out in flat space. Mappings of squashed 4D spheres into flat space are avoided. This point of view, which was summarized in a previous publication,[15] will be developed here in detail.

To clarify the statistical mechanics of disclination lines in 3D flat space, we have found it helpful to consider analogous defect descriptions of liquids in two dimensions. Here, analytical theories of freezing are possible,[16,17] based on defect-pairing ideas suggested by Kosterlitz and Thouless.[18] The obvious analog of the icosahedron in two dimensions is a hexagon composed of six identical triangular packing units. Unlike the icosahedron, however, the hexagon can be periodically extended to tile the plane. To introduce frustration, one imagines that particles are packed in a space of constant negative curvature.[19] As shown in Fig. 1(b), cracks then open up between six particles symmetrically arranged around a central atom to form a hexagon. The free volume associated with these cracks tends to zero as space becomes flat.

The relationship between frustration and curvature in two and three dimensions is summarized in Fig. 2. When embedded in $S3$ the distance l between surface atoms in an icosahedron is related to the distance d to the center by (see Sec. III)

$$\cos(\kappa l)=1-(1-\sqrt{5}/5)\sin^2(\kappa d)\ , \tag{1.1}$$

where κ^{-1} is the radius of the sphere. The parameter d is the particle diameter for hard spheres, a typical interparticle spacing for softer potentials. When κ tends to zero, we recover the flat-space ratio

$$l/d=4/(10+2\sqrt{5})^{1/2}\approx 1.051\,462\ . \tag{1.2}$$

As illustrated in Fig. 2(a), one can adjust l/d to unity by taking

$$\kappa d=\kappa_* d=\cos^{-1}[\tfrac{1}{4}(1+\sqrt{5})]=0.628\,319\ . \tag{1.3}$$

The quantity κ_*^{-1} is the radius of the ideal tesselation of $S3$ and defines an intrinsic frustration length scale in 3D

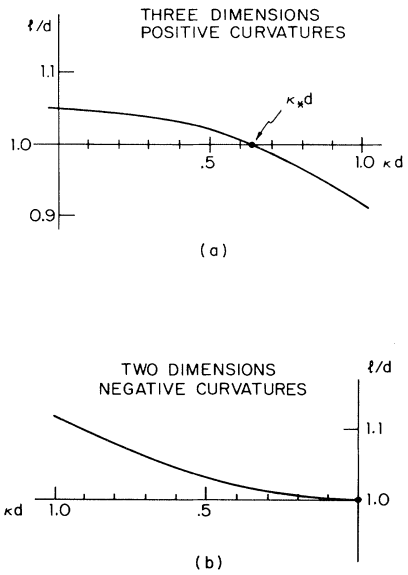

FIG. 2. Ratio l/d plotted as a function of the curvature parameter κd for (a) an icosahedron in $S3$ and (b) a hexagon in a space of constant negative curvature.

flat space. Distances in a two-dimensional (2D) space of constant negative curvature are determined by the metric in polar coordinates[9]

$$d^2s=d^2r+[\sinh(\kappa r)/\kappa]^2 d^2\phi\ , \tag{1.4}$$

where the parameter κ measures the deviation from flat space. Upon defining l and d as in Fig. 1(b), one finds a formula analogous to Eq. (1.1), namely[19]

$$\cosh(\kappa l)=1+\tfrac{1}{2}\sinh^2(\kappa d)\ . \tag{1.5}$$

As shown in Fig. 2(b), l exceeds d for $\kappa>0$, and one can mimic frustration in 3D flat space by choosing κd to be comparable to, say, the value in Eq. (1.3). Alternatively, one can take $\kappa d \ll 1$, and expand about the analytical theories of freezing[16,17] in flat space.

Figure 3 shows schematically a tangled mass of $\pm 72°$ disclination lines in a dense liquid in 3D flat space, regarded as a medium with a high degree of local

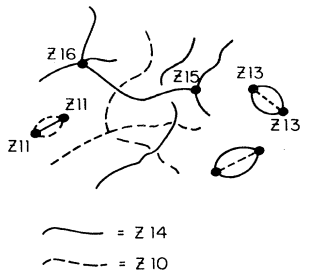

FIG. 3. Low-energy defect lines ($\pm 72°$ disclinations) in an icosahedral medium. Solid and dashed defect lines pass through particles with anomalous coordination numbers $Z\neq 12$. Particles not sitting directly on one of the lines have $Z=12$ icosahedral coordination shells.

icosahedral orientational order. As discussed in Sec. III, these lines carry SU(2) matrix "charges," which play a role analogous to the Burgers vectors carried by dislocations in a crystalline solid. The laws of combination for the lines are determined by SU(2) matrix multiplication: If two lines characterized by charges α and β come together at a node, the line which results is characterized by a charge[20]

$$\gamma=\alpha\beta\ . \tag{1.6}$$

The analogous rule for dislocations involves ordinary vector addition of the Burgers vectors.[21] Unlike the situation for dislocations, the matrix laws of combination for disclinations in an icosahedral medium are non-Abelian and depend on details of the way in which the defects are brought together.[20] One can, however, derive meaningful rules of combination for eight separate *classes* of defects. Equation (1.6) should be interpreted and saying that α and β combine to give a defect in the same class as γ. This interpretation removes the ambiguity associated with the order of matrix multiplication. At low temperatures, we expect the physics to be dominated by the class with the lowest energy, corresponding to rotations of $\pm 72°$ about one of the symmetry axes of the icosahedron. Figure 3 shows a representative sampling of the way in which these defect lines can be combined together. Isolated $\pm 72°$ disclination lines, which stop or start inside the medium, are impossible.

In two dimensions, liquids can be regarded as "hexatic" fluids interrupted by point disclinations, which are local points of five- and sevenfold symmetry in an otherwise sixfold medium.[16] The law of combination is given by addition of charges of, say, -1 and $+1$ associated with seven- and fivefold disclinations, respectively. A *microscopic* definition of point disclinations results from applying the Dirichlet construction to a 2D particle configuration[22] and looking for coordination numbers which deviate from six. This "5-7 construction" (which "triangulates" the medium by assigning a set of nonoverlapping bonds connecting neighboring particles) is a seductive way of thinking about the statistical mechanics of 2D materials.[23] The dislocation-disclination theory of 2D freezing can be formulated entirely in this purely topological way.[24] In a high-temperature liquid, one has a dense "plasma" of 5's and 7's, which must somehow pair to form a solid at temperatures. Dislocations in the solid are 5-7 disclination dipoles.

In Sec. III we describe an analogous microscopic construction for disclination lines in three dimensions, which generalizes early work by Frank and Kasper.[14] One first divides a particle configuration into tetrahedra via the Voronoi construction[22] and then considers the environment of each near-neighbor bond. Most bonds in a dense liquid will be surrounded by five tetrahedra. Links of plus and minus disclination lines are associated with four- and sixfold tetrahedral bipyramids, respectively. The way in which anomalous links combine to form various coordination shells corresponds to the "nodes" possible for disclinations in an icosahedral medium. One is led to a natural association between defect lines and lines of anomalous coordination number in a nominally 12-coordinated medium. This association is illustrated in Fig. 3, where, in particular, $\pm 72°$ disclination lines are associated with lines of coordination number $Z=10$ and 14 respectively. The "canonical Kasper polyhedra" (excluding the icosahedron), which are the building blocks of the Frank-Kasper phases, are nodes for $-72°$ lines, and are associated with coordination numbers 14–16.[14] The corresponding "antidefects," formed from links of $+72°$ disclination line, have coordination numbers 10, 9, and 8, and display coordination shells which are canonical "hole" polyhedra discussed by Bernal.[22,25] When these holes are filled with metalloid atoms, one arrives at structures which are believed to be quite common in metallic glasses.[26]

As discussed above, we would like to regard supercooled liquids and metallic glasses as defected icosahedral liquid crystals with, however, a global excess of defects with a particular sign due to the curvature incommensurability. In a 2D space of constant negative curvature, the excess is fixed by the curvature and surface area per particle. Indeed, a straightforward consequence of the Gauss-Bonnet theorem is that the average coordination number $\bar{Z}$ exceeds six,[19,27]

$$\bar{Z}=6+3s\kappa^2/\pi\ , \tag{1.7}$$

where s is the surface area per particle. Evidently, there is a curvature-induced excess of sevenfold disclinations, in contrast to 2D flat space, where there are equal numbers of 5's and 7's. The corresponding quantity in three dimensions is the average number of tetrahedra $\bar{q}$ packed around each bond. Although the curvature incommensurability of flat space forces this quantity to exceed 5, the value for an icosahedron, the deviation from 5 is, in general, sensitive to the details of the particle packing. It is possible, however, to define an *ideal* tetrahedral flat-space packing via a relaxation process into the fourth dimension. Subject to some plausible assumptions, we find that on the surface of a sphere $S3$ with radius κ^{-1} the ideal value of $\bar{q}$ is (see Sec. III)

$$\bar{q}_{\text{ideal}}(\kappa)=\frac{2\pi-3\kappa^2 v/d}{\cos^{-1}(\frac{1}{3})-\frac{1}{2}\kappa^2 v/d}\ , \tag{1.8a}$$

where v is the volume per particle and d is the particle separation determined by the pair potential. Although there are small corrections to this formula for finite κ due to the finiteness of the space (of order 0.05% when $\kappa=\kappa_*$), we expect that it becomes exact in the flat-space limit $\kappa\to 0$, where

$$\bar{q}_{\text{ideal}}=2\pi/\cos^{-1}(\tfrac{1}{3})\approx 5.104\,299\ \ \text{(flat space)}\ . \tag{1.8b}$$

This result is identical to one obtained for a "statistical honeycomb" model by Coxeter in 1958.[7] The value of $\bar{q}$ in the Frank-Kasper phases with large unit cells agrees with Eq. (1.8b) to within a few parts in 10^4 (see Table IV). There appears to be a systematic decrease of $\bar{q}$ towards $\bar{q}_{\text{ideal}}$ when dense-random-packing models are relaxed in a soft potential. We expect that a similar decrease occurs in liquids cooled below the equilibrium melting temperature. In this sense the Frank-Kasper phases, if one ignores their crystallinity, approximate an "ideal glass."[28]

In 3D spaces with arbitrary curvature, the average coordination number $\bar{Z}$ is related to $\bar{q}$ by[22]

$$\bar{Z}=12/(6-\bar{q}) , \tag{1.9}$$

which gives $\bar{Z}_{\text{ideal}}=13.397$ in flat space. The icosahedral coordination $\bar{Z}=12$ is recovered when $\bar{q}=5$. Although it is possible to force $\bar{q}$ to be six by working in a hyperbolic space, note from (1.9) that the corresponding coordination number *must be infinite*. Note also that in three dimensions it is q, rather than the coordination number, which plays a fundamental role.

The disclination lines shown in Fig. 3 should be contrasted with the "odd lines" defined by Rivier.[20] Rivier's lines thread odd-membered rings in Voronoi polyhedra. The only thing conserved along them is their "oddness." Although the odd lines may be useful in understanding in covalently bonded materials, they are in our view an awkward way to describe simple liquids and metallic glasses. Since 12 odd lines meet at the center of every icosahedron, such "lines" would have to *fill all the empty space* in Fig. 3. Icosahedral disclination lines thread rings in Voronoi polygons whose coordination *differs* from 5. At low temperatures, the anomalous ring coordinations four and six dominate, and are conserved along plus and minus disclination lines, respectively. Following speculations by Anderson,[29] Rivier has argued that the singular behavior of transport coefficients in supercooled liquids is associated with a Kosterlitz-Thouless disclination pairing transition.[30] A sharp pairing transition seems unlikely, however, because of the excess $-72°$ disclinations produced by the curvature incommensurability. Indeed, barring cooperative phenomena associated with rearrangements of these lines, one might expect the glass transition to be gradual with simple Arrehenius divergences in transport coefficients at sufficiently low temperature. Our point of view also differs from interesting work by Ninomiya, who regards glasses as a mixture of four-particle tetrahedra and six-particle octahedra.[31] Although the Voronoi construction used here is ambiguous for assigning near-neighbor bonds within a perfect octahedron, an infinitesimal perturbation allows a unique decomposition into four distorted tetrahedra.

Toulouse has commented on the analogy between frustration in spin-glasses and the effect of parallel transport on vectors in curved space.[32] The picture of frustration in real glasses developed here is in fact closely related to "uniformly frustrated" spin-glass models.[33,34] XY spins on a square lattice described by the nearest-neighbor Hamiltonian

$$H=-J\sum_{\langle i,j\rangle}\cos(\theta_i-\theta_j-f_{ij}) \tag{1.10}$$

provide one of the simplest such models. Here, θ_i is the angle each spin makes with some reference axis, and the frustration is the same for every elementary plaquette P,

$$f_{12}^{P}+f_{23}^{P}+f_{34}^{P}+f_{41}^{P}=f_0 . \tag{1.11}$$

The frustration ensures an excess of Kosterlitz-Thouless vortices with a particular sign, and the model provides a description of superconducting films in a perpendicular magnetic field.[34] Provided the excess vortex density is low ($f_0 \ll 1$), so that the discreteness of the lattice can be neglected, this model is similar locally to liquids on surfaces of constant negative curvature, except that disclinations play the role of vortices. A heuristic argument leading to an analogous model for the frustration associated with icosahedra in flat space is given in Sec. III. The uniformity of the frustration in these models is a consequence of the unformity of space.

Order and frustration in 2D liquids are discussed in Sec. II. We urge readers primarily interested in three dimensions to at least skim this section since it will be used to illustrate a number of concepts useful in three dimensions. In addition to liquids in spaces of constant negative curvature,[35] we shall discuss the finite icosahedral tiling of the positively curved surface of a 3D sphere $S2$ by 12 particles. The homotopy (rules of combination) for defects in this space turns out to be identical to the homotopy for rotational line defects in a 3D icosahedral medium. When more than 12 particles are packed into $S2$, the resulting incommensurability mimics 3D flat-space frustration, except that it occurs on a finite manifold.[13] Results for 3D flat space will be derived in Sec. III. In addition to discussing how to parametrize order and frustration, we describe macroscopic and microscopic ways of thinking about icosahedral disclination lines. We emphasize the important role played by the Frank-Kasper phases and speculate on the behavior of disclination lines in melts near the glass transition. The relevance of Eq. (1.8a) to computer simulations of particles embedded in $S3$ is discussed as well. The homotopy group for disclination lines in cubic liquid crystals is discussed in Appendix A. These defects play a role in tilings of $S3$ which are incommensurate with another, 8-particle, cuboctahedral regular polytope discussed by Coxeter.[8,9] They also occur in materials with cubic bond orientational order[36] in 3D flat space. Finally, in Appendix B we compare the disclination lines in metallic glasses and the Frank-Kasper phases with proposals for similar structures in the blue phases of cholesteric liquid crystals.[37,38]

II. TWO DIMENSIONS

A. Defects in flat space

We are beginning to develop a fairly detailed theoretical and experimental understanding of liquids cooled on flat, 2D surfaces.[39] Although first-order freezing transitions are certainly possible, liquids can also freeze via a sequence of two continuous phase transitions.[40] To understand this latter possibility, it is necessary to make a distinction between translational and orientational order. In contrast to crystalline solids, which display both kinds of order, phases of matter with no translational order, but with extended correlations in the orientations of local crystallographic axes (defined by clusters of near-neighbor bonds) are possible.

Figure 4 shows the result of carrying out the Dirichlet construction in a computer simulation of a dense liquid, and in a solid at a lower temperature.[41] The anomalous 5- and 7-coordinated particles, shown as asterisks and diamonds, can be viewed as microscopically defined point

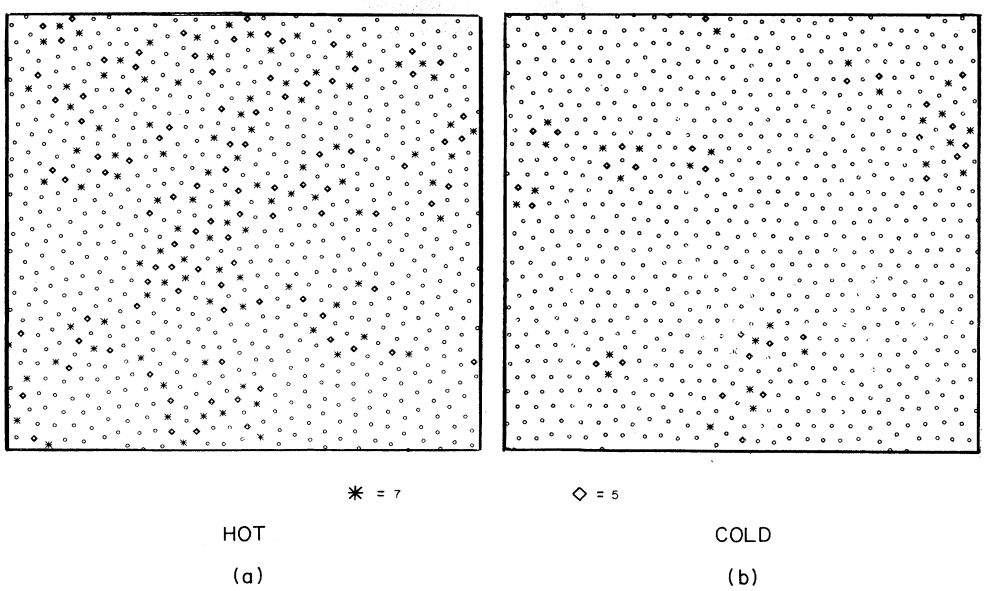

FIG. 4. Computer-simulation "snapshots" of (a) hot and (b) cold arrays of particles. Dirichlet construction has been used to highlight 7- (*) and 5- (◇) coordinated particles.

disclinations. Clearly, the 5's and 7's in the high-temperature "plasma" phase must somehow annihilate to form the low-temperature solid. This can happen abruptly, via a first-order transition, or more gradually, via a two-stage pairing process.[16] In the latter scenario, disclinations first pair to form 5-7 dipoles at a liquid-to-hexatic transition temperature T_i. These dipoles can be regarded as dislocations with a Burgers vector related to the dipole moment by a 90° rotation.[24] The dislocations then pair at a lower temperature T_m to form a crystalline solid.

Both of the pairing transitions discussed above can be continuous, with the latent heat one usually associates with freezing spread out over an intermediate hexatic phase. The hexatic phase differs from an ordinary fluid due to an extra term in its long-wavelength free energy, namely

$$F=\tfrac{1}{2}K_A\int |\vec{\nabla}\theta(\vec{r})|^2 d^2r \ . \tag{2.1}$$

Here, $\theta(\vec{r})$ is the angle a near-neighbor bond makes in respect to some reference axis, modulo 60°. A nonzero stiffness constant K_A in Eq. (2.1) means that hexatics behave in many respects like sixfold liquid crystals. A useful measure of the degree of hexatic order in an isotropic liquid is the order parameter[16]

$$\psi_6(r)=\exp[6i\theta(r)] \ . \tag{2.2}$$

An orientational correlation length $\xi_6(T)$ can be defined via the decay of

$$G_6(r)\equiv\langle\psi_6^*(\vec{r})\psi_6(\vec{0})\rangle\sim e^{-r/\xi_6(T)} \ . \tag{2.3}$$

Near the disclination pairing transition, $\xi_6(T)$ diverges,[16]

$$\xi_6(T)\sim\exp(\text{const}/|T-T_i|^{1/2}) \ . \tag{2.4}$$

Both dislocation and disclination point defects are possible in 2D crystals. Formally, one says that the stable point defects are given by the homotopy group[20]

$$\pi_1([T_2\times\mathrm{SO}(2)]/(t_2\times C_6)) \ . \tag{2.5}$$

Here, $T_2\times\mathrm{SO}(2)$ represents the semidirect product of translational (T_2) and rotational [SO(2)] symmetry groups of an isotropic liquid, and $t_2\times C_6$ signifies the corresponding discrete symmetry groups of a hexagonal-close-packed solid. According to Mermin,[20] there are at present unresolved difficulties in using homotopy theory in this way. In this paper, we shall ultimately sidestep such issues by regarding disclinations as the fundamental defects at *all* temperatures. A set of disclinations can be uniquely associated with every particle configuration using the Dirichlet construction. The standard defects in a crystalline solid are then regarded as composite objects.[23] Two dislocations, represented by 5-7 disclination dipoles, appear in the upper right corner of Fig. 4(b). Three such dislocations, when arranged in a configuration with no net dipole moment, can be used to represent vacancies and interstitials. Grain boundaries are linear arrangements of the form —5-7—5-7—5-7—. A high-temperature liquid is simply a dense plasma of disclinations. As will be discussed in Sec. III this point of view has a natural generalization into three dimensions.

B. Negative curvatures

The 2D hyperbolic space $H2$ is defined by the metric in Eq. (1.4), where the frustration parameter κ is related to the Gaussian curvature K by[9]

$$\kappa=\sqrt{-K} \ . \tag{2.6}$$

Here, r and ϕ are polar coordinates which reduce to ordinary flat-space polar coordinates in the limit $\kappa\to 0$. It is straightforward to integrate the metric (1.4) and find the geodesic distance l_{ab} between two particles with polar

coordinates (r_a,ϕ_a) and (r_b,ϕ_b),

$$\cosh(\kappa l_{ab})=\cosh(\kappa r_a)\cosh(\kappa r_b) -\sinh(\kappa r_a)\sinh(\kappa r_b)\cos(\phi_a-\phi_b) . \quad (2.7)$$

Applying this formula to n particles ($n \geq 6$) symmetrically arranged around a central atom to form an n-fold regular polygon, we set $r_a=r_b=d$, $l_{ab}=l_n$, and $\phi_a-\phi_b=2\pi/n$, and find

$$\cosh(\kappa l_n)=1+[1-\cos(2\pi/n)]\sinh^2(\kappa d) , \quad (2.8)$$

which reduces to Eq. (1.5) for the special case of a hexagon. There is clearly an infinite sequence of special, "commensurate" curvatures κ_n such that an n-fold polygon can be decomposed into n equilateral triangles. Setting $l_n=d$ in Eq. (2.8), we find

$$\kappa_n d=\cosh^{-1}[\cos(2\pi/n)/(1-\cos(2\pi/n)] , \quad (2.9)$$

which gives $\kappa_6 d=0$, $\kappa_7 d=1.090\,55$, $\kappa_8 d=1.528\,57$, $\kappa_9 d=1.855\,08$, etc. As discussed in the Introduction, we shall be primarily interested in curvatures such that κ is intermedate between κ_6 and κ_7.

When the curvature is incommensurate, the free-energy Eq. (2.1) describing hexatic order must be modified at sufficiently long wavelengths. Indeed, it is difficult to measure all bond angles with respect to a common "reference axis" outside of flat space. The reference axis changes when parallel transported, and will not, in general, return to its initial value when carried around a closed path.[42,43] It is helpful to rewrite Eq. (2.1) in terms of a unit vector $\vec{n}(r)$ directed along a bond centered at $\vec{r}$,

$$F=\tfrac{1}{2}K_A\int(\partial_i n^j)^2 d^2r , \quad (2.10)$$

with the understanding that directions related by a 60° rotation are equivalent. A natural generalization into curved space is

$$F=\tfrac{1}{2}K_A\int(\partial_i n^j+\Gamma^j_{ki}n^k)^2\sqrt{g}\,d^2x , \quad (2.11)$$

where the Γ^j_{ki} are connection coefficients which allow for parallel transport,[42,43] and the element of area $\sqrt{g}\,d^2x$ is given by the determinant g of the metric tensor g_{ij}.[9] For the polar coordinates r and ϕ used above (with $d^2x=dr\,d\phi$), we have[9]

$$g=\det\begin{bmatrix}1 & 0\\ 0 & \sinh^2(\kappa r)/\kappa^2\end{bmatrix}=\sinh^2(\kappa r)/\kappa^2 . \quad (2.12)$$

If we work, instead, in a local Cartesian coordinate system (x^1,x^2) centered at the origin, it is straightforward to show that

$$g_{ij}=\delta_{ij}-\kappa^2 x^i x^j+O(x^4) \quad (2.13)$$

and

$$\Gamma^j_{ki}=-\kappa^2\delta_{ki}x^j+O(x^3) . \quad (2.14)$$

Equation (2.11) is reminiscent of the gradient free energy for a superconductor in flat space,[44]

$$F_s=\frac{\hbar^2}{2m}\int\left|\left(\vec{\nabla}-\frac{ie}{\hbar c}\vec{A}\right)\psi\right|^2 d^2r , \quad (2.15)$$

where $\psi(r)$ is the superconducting order parameter and $\vec{A}(r)$ is the vector potential. To make the connection explicit, set

$$\psi(\vec{r})\equiv n^1(\vec{r})+in^2(\vec{r}) , \quad (2.16)$$

and note that F_s may be reexpressed as

$$F_s=\frac{\hbar^2}{2m}\int\left[\partial_i n^j-\frac{e}{\hbar c}A_i\epsilon_{jk}n^k\right]^2 d^2r . \quad (2.17)$$

Comparing Eq. (2.17) with Eqs. (2.11) and (2.14), we see that a flat-space superconductor looks locally like a hexatic in a curved space with connection coefficients

$$\tilde{\Gamma}^j_{ki}=-\frac{e}{\hbar c}A_i\epsilon_{jk} , \quad (2.18)$$

where ϵ_{ij} is the 2×2 antisymmetric tensor $\epsilon_{xy}=-\epsilon_{yx}=1$. The curvature acts in some ways like a uniform magnetic field directed normal to the surface. Taking $A_i=\frac{1}{2}H\epsilon_{il}x^l$, corresponding to a uniform magnetic field of strength H, we see that both Γ^j_{ki} and $\tilde{\Gamma}^j_{ki}$ are linear in x, although their tensor structure is different. More precise connections of this kind are embodied in the fiber-bundle approach to gauge-field theories.[45]

According to Eq. (2.11) the free energy will be minimized when neighboring bonds are aligned after parallel transport to, say, the midpoint of the geodesic line joining them. It is impossible to make the covariant derivative in (2.11) vanish everywhere, however. Consider the effect of parallel transport of the bond vector $\vec{n}$ around the closed loop shown in Fig. 5. This operation can be viewed as an attempt to construct a field of "aligned" bond vectors. It is well known, however, that the resulting vector $\vec{n}$ will differ from $\vec{n}'$ by an amount[42]

$$\Delta n^k=-\tfrac{1}{2}R^k_{ilm}n^i\epsilon^{lm}a , \quad (2.19)$$

where a is the area of the loop and $\epsilon^{lm}=\epsilon_{lm}$. The quantity R^k_{ilm} is the 2D Riemann curvature tensor[42,43]

$$R^k_{ilm}=-\kappa^2(g_{il}\delta_{km}-g_{im}\delta_{kl}) . \quad (2.20)$$

With the use of the Cartesian form (2.13) for the metric tensor, it is straightforward to show that the angle between $\vec{n}$ and $\vec{n}'=\vec{n}+\Delta\vec{n}$ is

$$\Delta\theta\approx|\vec{n}\times\vec{n}'|=-\kappa^2 a+O[(\kappa^2 a)^3] . \quad (2.21)$$

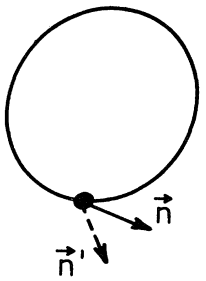

FIG. 5. Path around which the unit bond vector $\vec{n}$ is carried via parallel transport. On a curved surface $\vec{n}$ is carried into a different vector $\vec{n}'$ upon completing the closed circuit.

It is natural to associate this angular deficit with N_d disclinations of magnitude $-2\pi/6$ contained within the contour. The corresponding defect density is

$$n_d = N_d/a = 3\kappa^2/\pi \ . \tag{2.22}$$

Curvature forces disclinations into the material in the same way that a magnetic field forces Abrikosov flux vortices into a superconducting film with a large London penetration depth.[46] Note also the similarity between the closed loop in Fig. 5 and a frustrated plaquette in a spin-glass.

The curvature-induced excess disclinations rule out the possibility of extended hexatic order. To discuss what happens when such systems are cooled from high temperatures, we abandon the hydrodynamic description (2.11) and work directly with the Dirichlet construction.[19] When carried out in curved space, this procedure triangulates any particle configuration with a grid of geodesic near-neighbor bonds. According to the Gauss-Bonnet theorem, the integral Gaussian curvature of one of these geodesic triangles is[9]

$$\int_{\Delta_{ABC}} (-\kappa^2)\sqrt{g}\, d^2x = A + B + C - \pi \ , \tag{2.23}$$

where A, B, and C are the angles subtended by the vertices. Ignoring edge effects it is straightforward to show from (2.23) that the average coordination number $\bar{Z}$ is related to the curvature as in Eq. (1.6).[19] The more general analysis of Gaspard *et al.*,[27] which accounts for bonds at the boundaries, leads to the same result. The density of excess sevenfold disclinations predicted by this microscopic approach is

$$n_d = (\bar{Z} - 6)/s = 3\kappa^2/\pi \ , \tag{2.24}$$

in agreement with Eq. (2.22).

At high temperatures the excess sevenfold disclinations superimposed on a dense 5-7 plasma should be hardly noticeable. As a system cools, this excess will become important when sufficient numbers of 5's and 7's have paired. The liquid-to-hexatic transition, assuming this occurs in flat space, will be smeared when the flat-space correlation length (2.4) becomes comparable to the spacing between the excess disclinations with density n_d. A similar smearing of the Kosterlitz-Thouless vortex pairing transition occurs in superconducting films in the presence of an applied magnetic field.[46]

There are two possibilities in the limit of very low temperatures. If the kinetics of disclination motion are fast compared to the cooling rate, one might expect the excess disclinations to form a "crystalline" superlattice with a spacing d^* consistent with the sevenfold tesselation of space predicted by Eq. (2.9),

$$d^*\kappa = 1.090\,55 \ . \tag{2.25}$$

Such an "Abrikosov flux lattice" would be like the icosahedral arrangement of fivefold vertices embedded among many sixfold vertices in the positively curved surface of a geodesic dome. As we shall see, the Frank-Kasper phases represent a similar solution to the problem of frustration in 3D flat space. A soft interparticle potential would presumably be required to pack an integral number of particles into the superlattice interstices for arbitrary incommensurate curvatures $\kappa_6 < \kappa < \kappa_7$.

A second possibility is displayed in Fig. 6, which shows a particle configuration obtained via Bennett's packing algorithm[47] for hard disks with $\kappa d = 0.6$.[48] Figure 6 is a 2D analog of dense random packing. The coordination-number histogram in the inset shows that most particles have coordination number six with a curvature-induced asymmetry between the remaining 5's and 7's. The degree of disorder in the figure is presumably related to number of unpaired 5's. We would expect particle configurations like Fig. 6 when systems are cooled rapidly compared to the time necessary to equilibrate disclinations. We shall argue that metallic glasses provide an example of this second possibility in 3D flat space.

Unpaired disclinations have a drastic effect on translational order. Note from Fig. 7(a) that Burgers circuits around an isolated disclination fail to close by larger and larger amounts with increasing radius. As illustrated by the relaxed threefold disclination in a square lattice shown in Fig. 7(b),[49] this behavior can be associated with a cloud of unpaired dislocations surrounding every disclination. The separation between these dislocations defines an intrinsic translation correlation length ξ_T^0. It is straightforward to show that the intrinsic translational and orientational lengths possible in a system with incommensurate curvature are related by[19,49]

$$\xi_T^0 = (\xi_6^0 d)^{1/2} \ . \tag{2.26}$$

Here we have defined an intrinsic orientational correlation length ξ_6^0 by

$$\xi_6^0 = n_d^{-1/2} \ , \tag{2.27}$$

and ignored the possibility of commensurate superlattices. According to Eq. (2.26), translational order is broken up on a much finer scale than orientational order by the excess disclinations.

Measurements of shear viscosities in disordered particle configurations like Fig. 6 would be quite illuminating. In analogy with flat-space theories of liquid viscosities,[50] we expect that shear stresses relax at a rate proportional to the concentration of free dislocations, regarded as 5-7 disclination pairs. This dislocation density should be controlled by the small concentration of fivefold disclinations evident in Fig. 6. One might expect liquids cooled in metastable equilibrium to exhibit an Arrhenius divergence in the shear viscosity $\eta_s(T)$,

$$\eta_s(T) \sim e^{E_a/k_B T} \ , \tag{2.28}$$

where E_a is the activation energy of a 5-7 pair. It seems unlikely that isolated disclinations can relax shear stresses. If this point of view is correct, "glassy" particle configurations (consisting of a disordered array of excess sevenfold disclinations) could have essentially infinite viscosities.

There may also be a connection between unpaired disclinations and phonon localization. In the high-frequency ballistic limit one might expect phonon trajectories to follow the local crystallographic coordinate axes. As shown

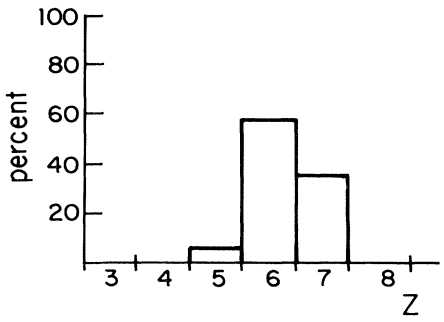

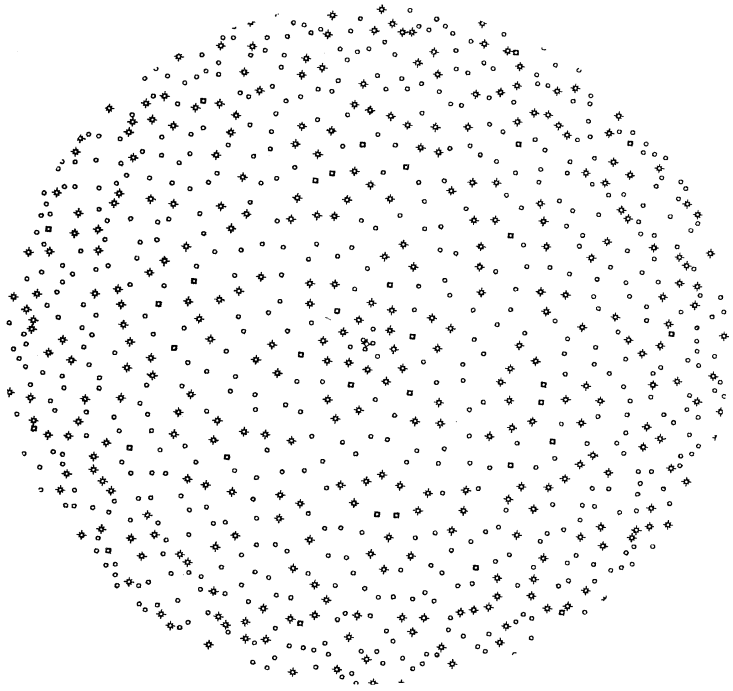

FIG. 6. Sequentially deposited hard disks projected out of a space of constant negative curvature. Successive disks with identical diameters ($\kappa d = 0.6$) are brought in so as to just touch the growing cluster at a point as close as possible to the center (see Ref. 48). Anomalous 7- (*) and 5- (◇) coordinated particles in this glassy configuration are highlighted. The same algorithm produces a hcp lattice in flat space. Histogram shows the asymmetry between 5's and 7's.

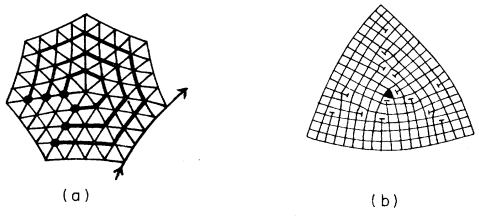

FIG. 7. (a) Sevenfold disclination in a triangular solid, together with Burgers circuits which fail to close by an amount which depends on their size. Trajectory marked with arrows shows how a ballistic phonon is deflected by the disclination. (b) Dislocation cloud surrounding a threefold disclination in a square lattice.

in Fig. 7(a), these trajectories are bent by disclinations the way light is bent when it passes near the sun. It seems plausible that phonons localize in a disordered medium at high frequencies (as seems to be the case in 3D flat space[51]) because of their inability to penetrate a random disclination array.

C. Positive curvatures

Flat space can, of course, also be made incommensurate by imposing a positive curvature. Virtually all the formulas in the preceding subsection can be taken over, with the replacement

$$\kappa^2 \rightarrow -\kappa^2 , \tag{2.29}$$

where κ^{-1} now represents the radius of the sphere $S2$. There are three commensurate positive curvatures, $\kappa_5 d = 1.107\,15$, $\kappa_4 d = \pi/2$, and $\kappa_3 d = \cos^{-1}(\frac{1}{3})$, corresponding to icosahedral, cuboctahedral, and tetrahedral tesselations of 12, 6, and 4 particles, respectively. Spaces of positive curvature are of course finite, and hence provide less insight into frustration in infinite 3D flat space than a space of constant negative curvature. The 12-particle tessellation of $S2$, however, is in many ways quite similar to the ideal 120-particle tessellation of $S3$ discussed in the Introduction.[13] It is of some interest to discuss defects in this simple space, and the role they play for positive curvatures such that $0 < \kappa < \kappa_5$.

Figure 8 shows the Dirichlet construction applied to 12 particles embedded in the surface of a sphere. The ground state for simple pair potentials is surely an icosahedral arrangement where every particle has five near neighbors. Figure 8 shows an excitation consisting of two 4-6 pairs. In analogy with flat-space configurations such as in Fig. 4(b), it is tempting to regard this excitation as a dislocation pair in an icosahedral "crystal." Isolated 4's and 6's would be viewed as disclinations. These ideas can be explored further by applying the defect homotopy theory summarized in the illuminating review article by Mermin.[20] This is a continuum approach which focuses on properties of large loops surrounding point defects. Its utility when applied to a finite space of 12 particles is certainly questionable. Nevertheless, insights not obvious using the more microscopic Dirichlet construction approach are possible. The same defect algebra applies, moreover, to icosahedral line defects in 3D flat space.

To make contact with flat-space formulas such as Eq. (2.5) it is convenient to decompose the symmetries of the surface of a sphere into "translational" and "rotational" parts. The set of translational motions possible for a point on a sphere may be denoted SO(3)/SO(2). The symmetry group of rotations about this point is SO(2). In an icosahedral solid, these combined symmetries [comprising the group SO(3)] are broken down to the discrete symmetries of the icosahedral point group Y. The homotopy group analogous to Eq. (2.5) is thus

$$\pi_1(\mathrm{SO}(3)/Y) \equiv Y' \,. \tag{2.30}$$

The 60 symmetry operations of the icosahedral point group are summarized in Fig. 9, which shows the six fivefold rotation axes, ten threefold rotation axes, and 15 twofold rotation axes of an icosahedron drawn in projection.

The homotopy group Y' of defects in this curved-space "crystal" is given by the lift of the icosahedral subgroup Y of SO(3) into SU(2).[20] The possible point defects are characterized by the symmetry operations of the perfect crystal. These in turn are labeled by a rotation axis $\hat{n}$ and an angle of rotation ω. Two SU(2) matrices,

$$U(\hat{n},\omega) = \exp(\tfrac{1}{2} i \omega \hat{n}\cdot\vec{\sigma}) = \cos(\tfrac{1}{2}\omega) + i \sin(\tfrac{1}{2}\omega)\hat{n}\cdot\vec{\sigma} \tag{2.31a}$$

and

$$U(\hat{n},\omega + 360^\circ) = -U(\hat{n},\omega) \,, \tag{2.31b}$$

are associated with each element of Y, where $\vec{\sigma}$ is the vector of Pauli matrices. When two defects characterized by matrices $U(\hat{n}_1,\omega_2)$ and $U(\hat{n}_2,\omega_2)$ combine, the resulting defect is described by the matrix

$$U(\hat{n},\omega) = U(\hat{n}_1,\omega_1)U(\hat{n}_2,\omega_2) \,. \tag{2.32}$$

It follows from (2.31a) and the properties of Pauli matrices that

$$\omega = 2\cos^{-1}[\cos(\tfrac{1}{2}\omega_1)\cos(\tfrac{1}{2}\omega_2) - \hat{n}_1\cdot\hat{n}_2 \sin(\tfrac{1}{2}\omega_1)\sin(\tfrac{1}{2}\omega_2)] \tag{2.33a}$$

and

$$\hat{n} = [\sin(\tfrac{1}{2}\omega_1)\cos(\tfrac{1}{2}\omega_2)\hat{n}_1 + \cos(\tfrac{1}{2}\omega_1)\sin(\tfrac{1}{2}\omega_2)\hat{n}_2 - \sin(\tfrac{1}{2}\omega_1)\sin(\tfrac{1}{2}\omega_2)\hat{n}_1\times\hat{n}_2]/\sin(\tfrac{1}{2}\omega) \,. \tag{2.33b}$$

Defects in the same homotopy class can be transformed into each other. When the defect α is carried around the defect β the resulting defect is[20]

$$\alpha' = \beta^{-1}\alpha\beta \,. \tag{2.34}$$

It is the *class* structure of the non-Abelian group Y' rather than the individual SU(2) matrix charges which determines how defects combine. The laws of defect combination are given by the class multiplication table of Y'. The

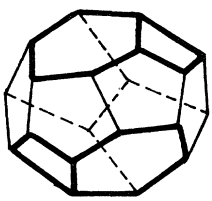

FIG. 8. Dirichlet construction applied to 12 particles embedded in the surface of a sphere. Heavy solid lines enclose two 4-6 pairs.

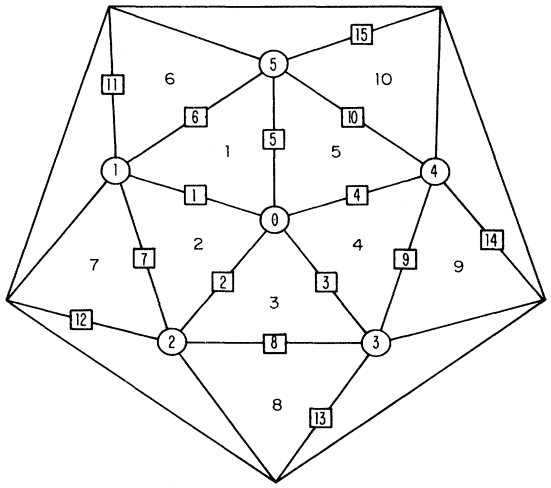

FIG. 9. Symmetry axes of an icosahedron drawn in projection about the fivefold symmetry axis labeled "0" at the origin. The vertex opposite "0" is not shown.

nine classes corresponding to the 120 elements of Y' are

$$\bar{\mathscr{C}}_0=\{1\}\ ,\quad \bar{\mathscr{C}}_0=\{-1\}\ ,$$
$$\mathscr{C}_5=\{U(\hat{n}_i,72°)\ ,U(\hat{n}_i,-72°),i=0,\ldots,5\}\ ,$$
$$\bar{\mathscr{C}}_5=\{U(\hat{n}_i,288°),U(\hat{n}_i,-288°),i=0,\ldots,5\}\ ,$$
$$\mathscr{C}_5^2=\{U(\hat{n}_i,144°),U(\hat{n}_i,-144°),i=0,\ldots,5\}\ ,$$
$$\bar{\mathscr{C}}_5^2=\{U(\hat{n}_i,216°),U(\hat{n}_i,-216°),i=0,\ldots,5\}\ ,$$
$$\mathscr{C}_3=\{U)\hat{m}_i,120°),U(\hat{m}_i,-120°),i=1,\ldots,10\}\ ,$$
$$\bar{\mathscr{C}}_3=\{U(\hat{m}_i,240°),U(\hat{m}_i,-240°),i=1,\ldots,10\}\ ,$$
$$\mathscr{C}_2=\{U(\hat{l}_i,188°),U(\hat{l}_i,-180°),i=1,\ldots,15\}\ ,$$

where $\hat{n}_i$, $\hat{m}_i$, and $\hat{l}_i$ denote five-, three-, and twofold rotation axes in Fig. 9. The class $\bar{\mathscr{C}}_0$ consists of a 360° rotation, while the classes $\mathscr{C}_5$, $\bar{\mathscr{C}}_5$, $\mathscr{C}_5^2$, and $\bar{\mathscr{C}}_5^2$ correspond respectively, to rotations of $\pm72°$, $\pm288°$, $\pm144°$, and $\pm216°$ about a fivefold symmetry axis upon traversing a closed counterclockwise path about a defect. The classes $\mathscr{C}_3$ and $\bar{\mathscr{C}}_3$ denote rotations of $\pm120°$ and $\pm240°$ about a threefold symmetry axis, while $\bar{\mathscr{C}}_2$ is composed of $\pm180°$ rotations about twofold rotation axes. The class $\mathscr{C}_0$ denotes configurations homotopic to the identity.

The symmetry elements in flat space analogous to the elements of Y' may be denoted $(\vec{b},e^{in\pi/3})$, where $\vec{b}$ denotes the Burgers vector of a dislocation and $e^{in\pi/3}$ denotes the rotation $\mathscr{R}_n$ associated with a disclination with charge n in, say, a triangular solid. As pointed out by Mermin, the conjugacy class of an elementary disclination $(\vec{0},e^{\pm i\pi/3})$ consists of defects of the form[20]

$$(\vec{b},e^{in\pi/3})(0,e^{\pm i\pi/3})(\vec{b},e^{in\pi/3})^{-1}=(-\mathscr{R}_n\vec{b}+\vec{b},e^{\pm i\pi/3})\ , \tag{2.35}$$

indicating that an isolated disclination in a triangular solid is in the same class as that disclination plus a dislocation with an arbitrary Burgers vector. The defect in Eq. (2.35) is the result of taking an elementary disclination, and then "translating" it to another position via the extra half-rows of atoms associated with a dislocation. Rotations of $\pm72°$ about a fivefold symmetry axis (corresponding to the class $\mathscr{C}_5$) play the role of elementary disclinations in a 2D icosahedral solid. In a way reminiscent of Eq. (2.35) the conjugate defects are simply $\pm72°$ rotations associated with translations to one of the other fivefold rotation axes of the icosahedron.

Table I shows the class multiplication table for Y'.[15] The classes appearing in a given entry summarize the possibilities which result when two classes are brought together.[20] Disclinations of $+72°$ and $-72°$ represent, respectively, the 4's and 6's shown in Fig. 8. Table I suggests that we can regard these defects as fundamental and regard all other defects as composite objects. Indeed, defects in any of the remaining classes can be obtained by forming judicious combinations of $\pm72°$ disclinations. The 5's and 7's in Fig. 4 play a similar role. It seems reasonable that 4's and 6's can continue to be regarded as the fundamental excitations when more than 12 particles are packed into $S2$ to obtain an incommensurate tesselation. Indeed, the 14-, 15-, and 16-particle coordination shells of the canonical Kasper polyhedra discussed in Sec. III B form a kind of Abrikosov flux lattice of 6's embedded in a matrix of 12 5's. We shall view microscopically

TABLE I. Class multiplication table for the group Y'.

$\mathscr{C}_0$	$\bar{\mathscr{C}}_0$	$\mathscr{C}_5$	$\bar{\mathscr{C}}_5$	$\mathscr{C}_5^2$	$\bar{\mathscr{C}}_5^2$	$\mathscr{C}_3$	$\bar{\mathscr{C}}_3$	$\mathscr{C}_2$
$\mathscr{C}_0$	$\bar{\mathscr{C}}_0$	$\bar{\mathscr{C}}_5$	$\mathscr{C}_5$	$\bar{\mathscr{C}}_5^2$	$\mathscr{C}_5^2$	$\bar{\mathscr{C}}_3$	$\mathscr{C}_3$	$\mathscr{C}_2$
$\mathscr{C}_5$		$12\mathscr{C}_0+5\mathscr{C}_5$ $+\mathscr{C}_5^2+3\mathscr{C}_3$	$12\bar{\mathscr{C}}_0+5\bar{\mathscr{C}}_5$ $+\bar{\mathscr{C}}_5^2+3\bar{\mathscr{C}}_3$	$\mathscr{C}_5+\bar{\mathscr{C}}_5^2$ $+3\mathscr{C}_3+2\mathscr{C}_2$	$\bar{\mathscr{C}}_5+\mathscr{C}_5^2$ $+3\bar{\mathscr{C}}_3+2\mathscr{C}_2$	$5\mathscr{C}_5+5\mathscr{C}_5^2$ $+3\mathscr{C}_3+2\mathscr{C}_2$	$5\bar{\mathscr{C}}_5+5\bar{\mathscr{C}}_5^2$ $+3\bar{\mathscr{C}}_3+2\mathscr{C}_2$	$5\mathscr{C}_5^2+5\bar{\mathscr{C}}_5^2$ $+3\mathscr{C}_3+3\bar{\mathscr{C}}_3+4\mathscr{C}_2$
$\bar{\mathscr{C}}_5$			$12\mathscr{C}_0+5\mathscr{C}_5$ $+\mathscr{C}_5^2+3\mathscr{C}_3$	$\bar{\mathscr{C}}_5+\mathscr{C}_5^2$ $+3\bar{\mathscr{C}}_3+2\mathscr{C}_2$	$\mathscr{C}_5+\bar{\mathscr{C}}_5^2$ $+3\mathscr{C}_3+2\mathscr{C}_2$	$5\bar{\mathscr{C}}_5+5\bar{\mathscr{C}}_5^2$ $+3\bar{\mathscr{C}}_3+2\mathscr{C}_2$	$5\mathscr{C}_5+5\mathscr{C}_5^2$ $+3\mathscr{C}_3+2\mathscr{C}_2$	$5\mathscr{C}_5^2+5\bar{\mathscr{C}}_5^2$ $+3\mathscr{C}_3+3\bar{\mathscr{C}}_3+4\mathscr{C}_2$
$\mathscr{C}_5^2$				$12\mathscr{C}_0+\bar{\mathscr{C}}_5$ $5\bar{\mathscr{C}}_5^2+3\mathscr{C}_3$	$12\bar{\mathscr{C}}_0+\mathscr{C}_5$ $+5\mathscr{C}_5^2+3\bar{\mathscr{C}}_3$	$5\bar{\mathscr{C}}_5+5\bar{\mathscr{C}}_5^2$ $+3\bar{\mathscr{C}}_3+2\mathscr{C}_2$	$5\bar{\mathscr{C}}_5+5\mathscr{C}_5^2$ $+3\bar{\mathscr{C}}_3+2\mathscr{C}_2$	$5\mathscr{C}_5+5\bar{\mathscr{C}}_5$ $+3\mathscr{C}_3+3\bar{\mathscr{C}}_3+4\mathscr{C}_2$
$\bar{\mathscr{C}}_5^2$					$12\mathscr{C}_0+\bar{\mathscr{C}}_5$ $+5\mathscr{C}_5^2+3\mathscr{C}_3$	$5\mathscr{C}_5+5\bar{\mathscr{C}}_5^2$ $+3\bar{\mathscr{C}}_3+2\mathscr{C}_2$	$5\bar{\mathscr{C}}_5+5\mathscr{C}_5^2$ $+3\bar{\mathscr{C}}_3+2\mathscr{C}_2$	$5\mathscr{C}_5+5\bar{\mathscr{C}}_5$ $+3\mathscr{C}_3+3\bar{\mathscr{C}}_3+4\mathscr{C}_2$
$\mathscr{C}_3$						$20\mathscr{C}_0+5\mathscr{C}_5$ $+5\bar{\mathscr{C}}_5^2+6\mathscr{C}_3$ $+\bar{\mathscr{C}}_3+4\mathscr{C}_2$	$20\bar{\mathscr{C}}_0+5\bar{\mathscr{C}}_5$ $+5\mathscr{C}_5^2+6\bar{\mathscr{C}}_3$ $+\mathscr{C}_3+4\mathscr{C}_2$	$5\mathscr{C}_5+5\bar{\mathscr{C}}_5$ $+5\mathscr{C}_5^2+5\bar{\mathscr{C}}_5^2$ $+6\mathscr{C}_3+6\bar{\mathscr{C}}_3+4\mathscr{C}_2$
$\bar{\mathscr{C}}_3$							$20\bar{\mathscr{C}}_0+5\bar{\mathscr{C}}_5$ $5\bar{\mathscr{C}}_5^2+6\mathscr{C}_3$ $+\bar{\mathscr{C}}_3+4\mathscr{C}_2$	$5\mathscr{C}_5+5\bar{\mathscr{C}}_5$ $+5\mathscr{C}_5^2+5\bar{\mathscr{C}}_5^2$ $+6\mathscr{C}_3+6\bar{\mathscr{C}}_3+4\mathscr{C}_2$
$\mathscr{C}_2$								$30\mathscr{C}_0+30\bar{\mathscr{C}}_0+10\mathscr{C}_5$ $+10\bar{\mathscr{C}}_5+10\mathscr{C}_5^2+10\bar{\mathscr{C}}_5^2$ $+6\mathscr{C}_3+6\bar{\mathscr{C}}_3+4\mathscr{C}_2$

TABLE II. Sixth-rank spherical harmonics used to define the icosahedral order parameter (3.1).

$$Y_{6m}(\theta,\phi)=\left[\frac{13}{4\pi}\frac{(6-|m|)!}{(6+|m|)!}\right]^{1/2}P_6^{|m|}(\cos\theta)e^{im\phi}\times\begin{cases}(-1)^m, & m\geq 0\\ 1, & m<0\end{cases}$$

$m=-6,-5,\ldots,+6$

$P_6^0(x)=\frac{1}{16}(231x^6-315x^4+105x^2-5)$

$P_6^1(x)=(1-x^2)^{1/2}\frac{21}{8}(33x^5-30x^3+5x)$

$P_6^2(x)=(1-x^2)\frac{105}{8}(33x^4-18x^2+1)$

$P_6^3(x)=(1-x^2)^{3/2}\frac{105}{2}(33x^3-9x)$

$P_6^4(x)=(1-x^2)^2\frac{945}{2}(11x^2-1)$

$P_6^5(x)=(1-x^2)^{5/2}10\,395x$

$P_6^6(x)=(1-x^2)^3 10\,395$

defined *lines* of four- and sixfold symmetry in a very similar way in 3D flat space.

III. THREE DIMENSIONS

A. Order and frustration

Icosahedral bond orientational order has been explored in bulk supercooled liquids and glasses by Steinhardt *et al.*[5] With every near-neighbor bond (defined, e.g., via the Voronoi construction[22]) we associate the set of $l=6$ spherical harmonics compiled in Table II,

$$Q_{6m}(\vec{r})=Y_{6m}[\theta(\vec{r}),\phi(\vec{r})]\ , \tag{3.1}$$

where $\theta(\vec{r})$ and $\phi(\vec{r})$ are the polar angles of the bond measured with respect to an external coordinate system. A rotationally invariant icosahedral correlation function analogous to Eq. (2.3) is[5]

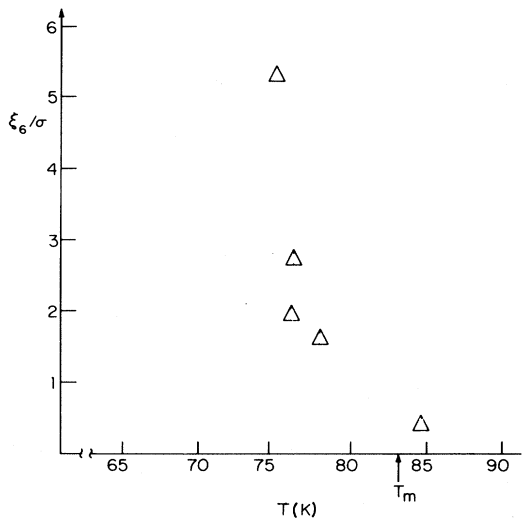

FIG. 10. Icosahedral correlation length for the supercooled Lennard-Jones system studied in Ref. 5. Temperature is displayed in units appropriate to supercooled argon, and σ locates the minimum in the pair potential. Equilibrium melting temperature for this constant-density simulation is indicated by the arrow.

$$G_6(r)=\frac{4\pi}{13}\sum_{m=-6}^{6}\langle Q_{6m}(\vec{r})Q_{6m}^*(\vec{0})\rangle\ . \tag{3.2}$$

The range of $G_6(r)$ measures the degree of alignment of neighboring icosahedra. In a high-temperature isotropic liquid, $G_6(r)$ decays exponentiall to zero, i.e., and $G_6(r)$ $\sim\exp(-r/\xi_6)$, where the orientational correlation length $\xi_6(T)$ is comparable to an interparticle spacing. As shown in Fig. 10, $\xi_6(T)$ increases with decreasing temperatures in a supercooled Lennard-Jones liquid until it becomes comparable to the 864-particle system size at about 10% below the equilibrium melting temperature.[5]

One also expects icosahedra in metallic glasses. As illustrated in Fig. 11, icosahedral coordination shells lead naturally to peaks at σ, 1.62σ, and 1.9σ in the radial distribution function,[52] where σ is the nearest-neighbor distance. These distances are consistent with the split second-peak structure observed via x-ray scattering in the radial distribution function of, for example, amorphous Co-P.[1] Correlations among icohsahedra in some standard models of metallic glasses were analyzed in Ref. 5. Although only modest correlations appear in relaxed Finney dense-random-packing models, there are rather striking correlations in alternative amorphon cluster models[6] of glass structure.

A question left open in Ref. 5 is the extent to which frustration inhibits extended icosahedral correlations. The largest orientational correlation length we can reliably read off Fig. 10 is only $\sim$3–5 particle diameters. An intrinsic frustration length scale can be extracted by referring to the ideal tessellation of $S3$.[7–9] Points $\vec{x}$ on the surface of a 4D sphere of radius κ^{-1} are conveniently parametrized using polar coordinates,

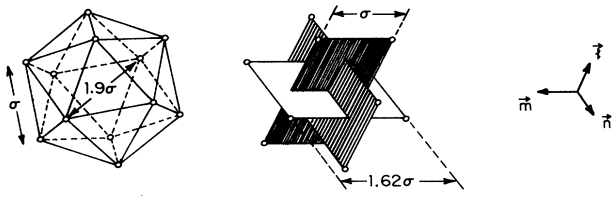

FIG. 11. Nearest-neighbor and next-nearest-neighbor distances in an icosahedron. Orthonormal triad $(\vec{l},\vec{m},\vec{n})$ associated with an icosahedron with this orientation is also shown.

$$\kappa\vec{x}=[\cos\phi\sin\theta\sin(\kappa r),\sin\phi\sin\theta\sin(\kappa r),\cos\theta\sin(\kappa r),\cos(\kappa r)]\ , \tag{3.3}$$

where (r,θ,ϕ) play a role similar to ordinary polar coordinates in flat space. It is easy to show using this 4D embedding of $S3$ that the geodesic distance l_{ab} between two points (r_a,θ_a,ϕ_a) and (r_b,θ_b,ϕ_b) is given by

$$\cos(\kappa l_{ab})=\cos(\kappa r_a)\cos(\kappa r_b)+\sin(\kappa r_a)\sin(\kappa r_b)[\cos\theta_a\cos\theta_b+\sin\theta_a\sin\theta_b\cos(\phi_a-\phi_b)]\ . \tag{3.4}$$

The 20 tetrahedra in a symmetric, icosahedral cluster of 13 particles divide the 4π of solid angle surrounding the central particle into 20 equal pieces. This is true in both flat and curved space. It follows that angles between the 12 radial bonds are the same in $S3$ as in flat space. Thus, we can take for angular coordinates of two neighboring radial bonds $(\theta_a,\phi_a)=(0,0)$ and

$$(\theta_b,\phi_b)=(\cos^{-1}[(1+3\sqrt{5}/5)/2],0)\ ,$$

just as in flat space.[53] If the length of the bonds is d, we find from Eq. (3.4) that the geodesic distance between the surface atoms l is related to d as in Eq. (1.1) in the Introduction. The frustration length scale associated with Eq. (1.3) is very short,

$$\kappa_*^{-1}=1.591\,549d\ . \tag{3.5}$$

Based on the discussion of 2D incommensurate curvatures in Sec. II, it seems unlikely that the icosahedral orientational correlation length ξ_6 can be more than a few times this intrinsic length scale.

The icosahedral order which *does* occur in supercooled liquids and metallic glasses is more complicated. Slowly varying icosahedral order at low temperatures can be specified by a position-dependent orthonormal triad of unit vectors $[\vec{l}(\vec{r}),\vec{m}(\vec{r}),\vec{n}(\vec{r})]$. A convention for relating these unit vectors to the orientation of a locally defined icosahedron is shown in Fig. 11. In the absence of frustration, we would expect a coarse-grained free energy similar to one discussed for cubic bond order in Ref. 36. In a "one-Frank-constant" approximation, this takes the form[36]

$$F=\tfrac{1}{2}K_A\int(|\vec{\nabla}\vec{l}|^2+|\vec{\nabla}\vec{m}|^2+|\vec{\nabla}\vec{n}|^2)d^3r\ . \tag{3.6}$$

In analogy with Eq. (2.17) we try to model the frustration discussed in the first paragraph of this paper by modifying the gradients, making, for example, the replacement

$$\partial_i l^j\rightarrow\partial_i l^j-M^j_{ik}l^k\ . \tag{3.7}$$

If the model is embedded in $S3$, we must also introduce connection coefficients,

$$\partial_i l^j\rightarrow\partial_i l^j-M^j_{ik}l^k+\Gamma^j_{ki}l^k\ . \tag{3.8}$$

In a local Cartesian-coordinate system (x^1,x^2,x^3), the metric tensor is[42]

$$g_{ij}=\delta_{ij}+\kappa^2x^ix^j+O((\kappa x)^4)\ , \tag{3.9}$$

and the connection coefficients are[54]

$$\Gamma^j_{ki}=\kappa^2\delta_{ik}x^j+O(\kappa^4x^3)\ . \tag{3.10}$$

The requirement that there be no frustration when the curvature assumes its commensurate value κ_* determines the matrix vector potential in Eq. (3.7) to lowest order in x,

$$M^j_{ik}\approx\kappa_*^2\delta_{ik}x^j\ . \tag{3.11}$$

A model for frustrated icosahedral order in flat space is thus

$$F=\tfrac{1}{2}K_A\int\sum_{\alpha=1}^{3}(\partial_i n^j_\alpha-M^j_{ik}n^k_\alpha)^2d^3r\ , \tag{3.12}$$

where M^j_{ik} given by (3.11), and where we have introduced the notation

$$\vec{n}_1=\vec{l},\ \ \vec{n}_2=\vec{m},\ \ \vec{n}_3=\vec{n}\ . \tag{3.13}$$

Defects must be introduced because it is impossible to make the term in parentheses in Eq. (3.12) vanish everywhere. The defect concentration is determined by the "Riemann curvature tensor" associated with M^j_{ik},[42]

$$R^i_{klm}=\partial_l M^i_{km}-\partial_m M^i_{kl}+O(\kappa_*^4)\approx\kappa_*^2(\delta_{il}\delta_{km}-\delta_{im}\delta_{kl})\ . \tag{3.14}$$

Equation (3.12) bears some resemblance to the Ginzburg-Landau gradient free energy for an extreme type-II superconductor in a uniform magnetic field.[44] M^j_{ik} is like a vector potential. It is straightforward to construct a "soft-spin" version of Eq. (3.12), using the icosahedral Landau theory described in Ref. 5. Because an isotropic curvature incommensurability plays the role of a "magnetic field," we would expect the lines of singular flux run in all directions.

B. Defects

Defects in liquids with local icosahedral order are singular lines where the icosahedral part of $Q_{6m}(\vec{r})$ drops to zero. These can be understood by referring to the ideal tessellation of $S3$. The symmetry operations of a structureless 4D sphere comprise the rotation group SO(4). This can be decomposed into rotational and translational parts just as in our discussion of $S2$ in Sec. II C, where SO(4)/SO(3) and SO(3) represent translational and orientational symmetry operations acting on a reference point, respectively. The six generators of SO(4) are analogous to the six generators of translations and rotations in flat space. The 120-atom icosahedral "crystal" imposes discrete rotational and translational symmetries on SO(4).

We shall only discuss *rotational* defects. These disclination lines are a direct result of the inability of flat space to accommodate an icosahedral solid. Their algebra is described by the homotopy group

$$Y' = \pi_1(\mathrm{SO}(3)/Y) \ . \tag{3.15}$$

We expect that these defects are fundamental in the sense that they can be used as building blocks for composite translational defects analogous to dislocations in a flat-space crystalline solid. This assumption was checked explicitly for the icosahedral tessellation of $S2$ in Sec. II C. A microscopic geometrical construction for decomposing an arbitrary particle configuration into disclination lines will be given below. Orientational order in flat space will be decorrelated on a scale comparable to or smaller than the spacing between the disclinations induced by the curvature incommensurability. Translational order will be broken up on an even finer scale [just as in two dimensions; see Eq. (2.26)], which provides another reason for only discussing defects in the orientational part of the ideal tessellation of $S3$.

The properties and class multiplication table of the homotopy group Y' were discussed in Sec. II C. The class multiplication table again summarizes the defect-combination laws and now determines, in particular, the allowed nodes in networks of disclination lines. A typical network is shown in Fig. 3. The physics at low temperatures should be dominated by lines in the class $\mathscr{C}_5$, composed of $\pm 72°$ rotations about a fivefold symmetry axis. These appear as solid ($-72°$ rotations) and dashed ($+72°$ rotations) lines in Fig. 3. Other defects represent larger rotations, and will have higher energies. When more energetic defects are suppressed, the relevant entry in the class multiplication table (see Table I) is

$$\mathscr{C}_5 \times \mathscr{C}_5 \approx 12\mathscr{C}_0 + 5\mathscr{C}_5 \ . \tag{3.16}$$

The term proportional to $\mathscr{C}_0$ reflects the fact that the solid and dashed lines can annihilate each other provided the rotations are about the same axis. Note, however, that pairs of low-energy lines can combine to produce not only the identity, but also another low-energy line, which accounts for the three-line nodes in Fig. 3. Consider, for example, the bubbles terminating in points denoted $Z11$ and $Z13$ in Fig. 3. The SU(2) matrix multiplications which allow these nodes are

$$U(72°,\hat{n}_4)U(-72°,\hat{n}_0)U(72°,\hat{n}_1) = E \tag{3.17}$$

and

$$U(-72°,\hat{n}_1)U(72°,\hat{n}_0)U(-72°,\hat{n}_4) = E \ , \tag{3.18}$$

where the rotation axes $\hat{n}_4, \hat{n}_0$, and $\hat{n}_1$ are shown in Fig. 9, and E denotes the unit matrix. Similar matrix multiplications correspond to the three- and four-line $-72°$ disclination nodes shown in Fig. 3. Ignoring high-energy lines is similar to neglecting multiply charged four- and eightfold disclinations in 2D flat space. It is easy to show using Table I that these more exotic excitations can be regarded as bundles of appropriately chosen low-energy lines.

A *microscopic* construction for disclination lines in any 3D particle configuration is summarized in Fig. 12. Following early work by Frank and Kasper,[14] we first partition space into tetrahedra by assigning near-neighbor bonds via the Voronoi construction. Links of plus or minus disclination line are assigned to bonds depending on their local environment. A "disclination-free" bond is surrounded by five tetrahedra and plays a role analogous to the six-coordinated particles in two dimensions. The excitations analogous to 7's and 5's in two dimensions are the bonds surrounded by six and four tetrahedra. All bonds in the ideal tessellation of $S3$ are spindles for fivefold bipyramids, composed of perfect tetrahedra. Although bipyramids of perfect tetrahedra are impossible in flat space, less distortion is required for fivefold bipyramids than for four- and sixfold bipyramids. As discussed in Ref. 14, sixfold bipyramids require less distortion than fourfold ones. Other kinds of bipyramids represent more exotic excitations.

Frank and Kasper give a proof that a link of sixfold line cannot simply terminate at an atom whose remaining bonds are fivefold. Such an atom would have coordination number $Z = 13$.[14] (There are other ways to make coordination shells with $Z = 13$; see below.) It is easy to repeat the Frank-Kasper argument and show that a fourfold link terminating at a particle whose remaining bonds are fivefold (corresponding to $Z = 11$) is also impossible. Lines of six- and fourfold links are the microscopic analog $-72°$ and $+72°$ wedge disclination lines in an icosahedral medium.

A number of standard coordination polyhedra have simple representations in terms of this construction. The canonical Kasper polyhedra[14] are shown in Fig. 13 together with their representation as nodes for $-72°$ disclination lines. Upon filling the free volume at the surface of an icosahedron with an extra atom, one obtains a particle with $Z = 13$ characterized by ten fivefold bonds and one fourfold bond interposed between two sixfold ones. It is natural to suppose that $Z = 13$ atoms will often occur in pairs, terminating the bubbles of two solid lines and one dashed line shown in Fig. 3. A small bubble corresponds to an interstitial in the ideal icosahedral solid.

The antidefects of the canonical Kasper polyhedra, which are nodes of $+72°$ disclination line, are shown in Fig. 14. The resulting $Z = 10$, 9, and 8 coordination shells are the canonical hole polyhedra discussed by Bernal.[22,25] The antidefect of the bubble consisting of two $Z = 13$ atoms is formed by first removing one particle from an icosahedral coordination shell to form a $Z = 11$ coordination shell. The particle at the center then has eight five-

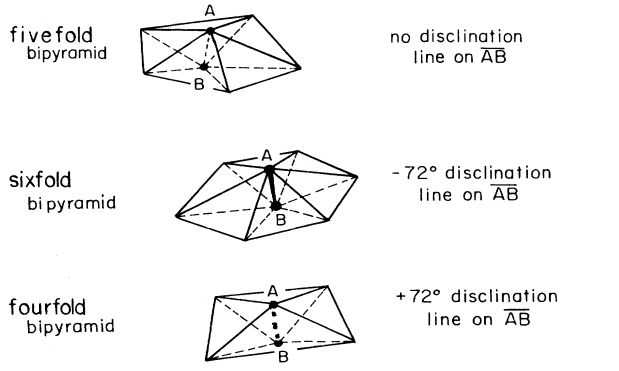

FIG. 12. Microscopic construction for disclinations in a medium composed of tetrahedra.

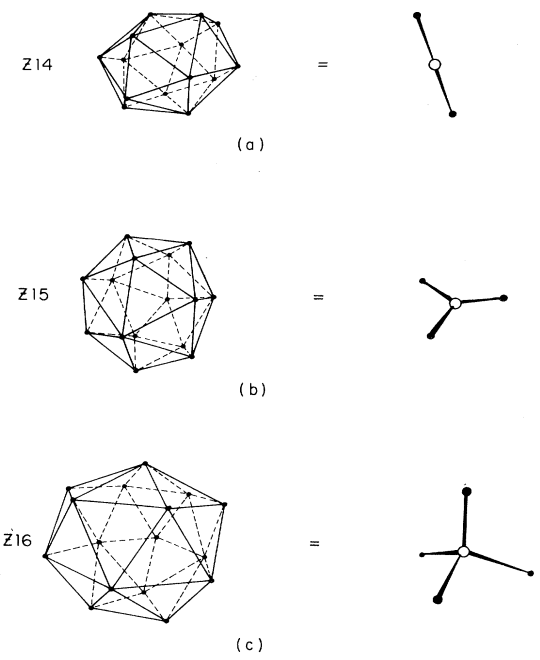

FIG. 13. Coordination shells of the canonical Kasper polyhedra together with their representation as links of $-72°$ disclination line. Open circles represent particles at the centers of the coordination shells.

fold bonds, together with a sixfold bond interposed between two fourfold ones. A bubble terminated by two $Z=11$ particles is shown in Fig. 3. A small bubble of this kind can be viewed as a vacancy in a perfect icosahedral solid.

In every case, the nodes for these geometrically defined disclination lines agree with the combination laws predicted by the homotopy group Y'. The $Z=13$ and 11 vertices, for example, are allowed by the SU(2) multiplications displayed in Eqs. (3.18). It is instructive to evaluate the bond spherical harmonics displayed in Table II for the $z=14$ and 10 particles discussed above. It is natural to take the z axis to be along the two links of disclination line in each case. Averaging over the bonds, one finds that icosahedral order parameter defined in Ref. 5 vanishes in the sense that only Q_{60} is nonzero, reflecting a purely uniaxial symmetry. Thus, lines of six- and fourfold bipyramids can be regarded as zeros in the icosahedral part of the order parameter in Eq. (3.1). By following the rotations of pentagonal bond spindles surrounding the two colinear sixfold bonds of a $Z=14$ Kasper polyhedron, one sees that these sixfold bonds are indeed segments of $-72°$ disclination line. A similar construction shows that the two colinear fourfold bonds in the $Z=10$ coordination polyhedron in Fig. 14 are segments of $+72°$ disclination line.

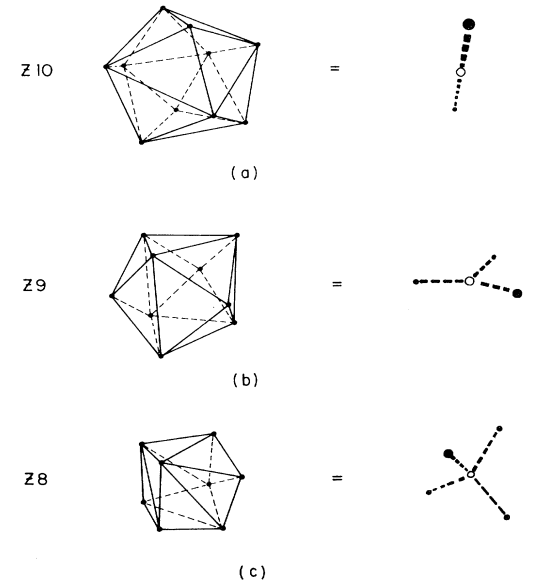

FIG. 14. Coordination shells associated with the canonical Bernal holes and their representation as links of $+72°$ disclination line. Open circles represent the particles which fill these holes.

C. Dense random packing and the Frank-Kasper phases

The microscropic defect construction described above can be applied to dense-random-packing models. Figure 15 shows the distribution of edges per face for Voronoi polygons in a dense-random-packing model[55] constructed by Ichikawa[56] for amorphous iron films using Bennett's packing algorithm.[47] Also shown are results for this model after relaxation in a soft potential.[55] It is easy to show that the number of edges on a particular face of a Voronoi polygon is the same as the number of tetrahedra surrounding the bond bisected by that face. Thus Fig. 15 is a direct measure of the distribution of defect line in the packing. As originally emphasized by Bernal,[25] fivefold bipyramids dominate in dense random packing. Note, however, that there are more links of sixfold than fourfold disclination line. This is a direct result of the curvature incommensurability, and is quite similar to the asymmetry between 7's and 5's displayed in Fig. 7. When the original model is relaxed. the number of fivefold bonds increases at the expense of the number of anomalous bonds. It is

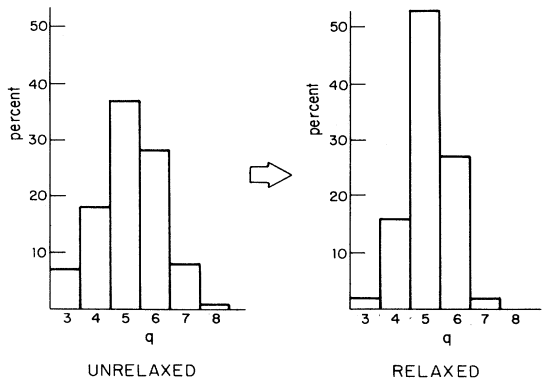

FIG. 15. Edge-per-face histograms for Voronoi polygons in the unrelaxed and relaxed Ichikawa-Bennett dense-random-packing model. Note the similarity with the histograms in Fig. 6.

TABLE III. Percentages of q-fold bonds in relaxed and unrelaxed Ichikawa-Bennett and Finney dense-random-packing models (all values in %).

	n_3	n_4	n_5	n_6	n_7	n_8
Unrelaxed Ichikawa-Bennett	7	18	37	28	8	1
Relaxed Ichikawa-Bennett	2	16	53	27	2	0
Unrelaxed Finney	5	19	40	29	6	1
Relaxed Finney	2	20	43	32	3	0
Liquid argon	7	20	36	27	8	2

tempting to regard the relaxation as an annihilation four- and sixfold links of disclination line. The more exotic three- and sevenfold links also participate in this pairing process.

Table III compares the results displayed in Fig. 15 with the same information for Finney's unrelaxed[57] and relaxed[58] ball-bearing dense-random-packing model. Although the changes are not as large as in the Bennett-Ichikawa model, the trend toward increasing the number of fivefold bonds is the same. It seems plausible that Bennett's model has more fivefold bonds (and hence more icosahedral order) because the method of construction is biased toward perfect tetrahedra.

A bcc crystal can also be analyzed in this way. Although there are no fivefold bonds, there is again an asymmetry in the eight sixfold and six fourfold bipyramids associated with every Wigner-Seitz cell. Every atom has coordination number $Z=14$. Close-packed fcc crystals are a special degenerate case. The existence of perfect cuboctahedra of six particles makes the assignment of bonds via the Voronoi construction ambiguous. There are similar ambiguities with the Dirichlet construction for square lattices in two dimensions. In both cases the ambiguity is removed by applying an infinitesimal shear stress. The coordination number of an fcc crystal then becomes 14, with the same fraction of six- and fourfold bonds as in the bcc case.

Because of the asymmetry between $-72°$ and $+72°$ disclination lines, the pairing process suggested by Fig. 15 cannot be carried to completion. There must be residual excess of unpairable sixfold bipyramids. This is precisely the situation found by Frank and Kasper in their pioneering study of complex alloy structures.[14] A number of crystalline phases with large unit cells, particularly in transition-metal alloys, consist of atoms with $Z=12$ icosahedral coordination shells interrupted by atoms with $Z=14$–16. The atoms with $Z>12$ combine to form a contiguous disclination network threading through an otherwise icosahedral medium. Table IV summarizes the properties of some typical Frank-Kasper phases. In $A15$ compounds the disclination network consists of three orthogonal grids of $Z=14$ atoms. The σ phase of, e.g., Co-Cr, consists of parallel lines of $Z=14$ atoms threading perpendicular planar networks of $Z=14$ and 15 particles, while the 162-atom unit cell of $Mg_{32}(Al,Zn)_{49}$ is dominated by a disclination network consisting of interconnected dodecahedra.

The information in Table IV is taken from the Frank-Kasper papers.[59] The average number of edges per face of the Voronoi polygons $\bar{q}$ in these phases was obtained from the average coordination number $\bar{Z}$ using the formula

$$\bar{q}=6-12/\bar{Z}. \tag{3.19}$$

This result follows directly from a generalized Euler relation for a network of Voronoi polygons quoted by Finney,[57] namely

$$\sum_i (6-i)F_i = 6(N_a+1)\ , \tag{3.20}$$

where F_i is the number of faces with i sides and N_a is the

TABLE IV. Distribution of 12-, 14-, 15-, and 16-coordinated particles in the Frank-Kasper phases.

Name	Examples	Atoms per unit cell	$Z=12$	$Z=14$	$Z=15$	$Z=16$	$\bar{Z}$	$\bar{q}$
$A15$	Nb_3Sn β-W	8	2	6	0	0	13.500	5.1111
Laves phase	Mg_2Zn_2	12	8	0	0	4	13.333	5.1000
μ phase	Fe_7W_6	13	7	2	2	2	13.385	5.1035
σ phase	Co-Cr β-U	30	10	16	4	0	13.467	5.1089
P phase	Mo-Ni	56	24	20	8	4	13.429	5.1064
—	$Mg_{32}Al_{49}$ $Mg_{32}Zn_{49}$	162	98	12	12	40	13.358	5.1017

total number of atoms. Upon defining

$$\bar{q}=\sum_i iF_i \Big/ \sum F_i \tag{3.21}$$

and neglecting unity relative to N_a on the right-hand side of (3.20), we have

$$6-\bar{q}=6N_a \Big/ \sum_i F_i \ . \tag{3.22}$$

If Z_j is the coordination number of the jth atom, we have

$$\sum_i F_i=\tfrac{1}{2}\sum_j Z_j \ , \tag{3.23}$$

since there are two atoms associated with every face. Equation (3.19) follows from (3.23) and (3.22) if we set

$$\bar{Z}=\sum_j Z_j/N_a \ . \tag{3.24}$$

Note from Table IV that $\bar{q}$ is always about 2% larger than five in the Frank-Kasper phases. This excess is a direct measure of the number of anomalous sixfold bonds.

D. Relaxation to an ideal glass

In two dimensions the number density of excess disclinations in a space of constant negative curvature is fixed by the topological constraint Eq. (2.24). In three dimensions the analogous quantity is $\bar{q}-5$. Although this deviation cannot, in general, be expressed in a compact form analogous to (2.24), it can be calculated exactly for a configuration we will call an ideal glass. Consider first an arbitrary array of identical particles interacting via a simple pair potential in 3D flat space. Although the bonds joining near neighbors divide space into tetrahedra, the curvature incommensurability ensures that not all tetrahedra will have equal edges. The strains embedded in disordered particle configurations can be relaxed by allowing motion into an extra dimension. The disclinations shown in Fig. 7, for example, could clearly lower their energy by buckling out of the 2D plane. Imagine a similar relaxation into a fourth dimension for 3D particle configurations under the constraint of constant coordination-number topology. No near-neighbor bonds, as defined by the Voronoi construction, can be broken. The result will be a crinkled 3D surface with local regions of positive and negative curvature. The bonds in this relaxed configuration will be more nearly equal than in the initial, flat arrangement. We define an ideal glass to be that configuration in flat space which is able to equalize all near-neighbor distances via the above relaxation process. Although the initial particle configuration is frustrated, the frustration is removed after relaxation since all particles then sit at the minima of their neighbors' pair potentials.

The value of $\bar{q}$ for this special configuration follows from a formula from the Regge calculus, namely[43]

$$\sum_j l_j\delta_j=\tfrac{1}{2}\int {}^{(3)}R\sqrt{g}\,d^3x \ , \tag{3.25}$$

where l_j is the length of the jth bond and the integral is over the scalar curvature ${}^{(3)}R$ of the 3D surface. The quantity δ_J is the deficit angle associated with the jth bond. The Regge calculus is a tetrahedral discretization procedure for integrals on curved manifolds, which becomes more and more accurate with increasing numbers of mesh points. The space enclosed by a tetrahedron is regarded as flat and the curvature is concentrated on the bonds.[43] For an ideal glass in flat space both the scalar curvature and all the deficit angles in Eq. (3.25) are zero. After relaxation, all the l_j are equal and the δ_j vary in sign and magnitude from bond to bond. We expect that the *integral* curvature, at least in the limit of very large system size, *remains* zero. The assumption is that in the initial flat-space integral curvature is encoded into the bond topology, and that as many regions of positive as negative curvature are generated by the relaxation process.

The angular deficit δ_5 associated with five perfect tetrahedra packed around a bond is shown in Fig. 16. This is the mismatch which results when the five tetrahedra are taken apart and reassembled into flat space. One clearly has

$$\delta_5=2\pi-5y \ , \tag{3.26}$$

where y is the dihedral angle of a perfect tetrahedron,

$$y=\cos^{-1}(\tfrac{1}{3}) \ . \tag{3.27}$$

The result for a j-fold bond is

$$\delta_j=2\pi-jy \ . \tag{3.28}$$

Inserting this result into Eq. (3.25), we have

$$2\pi d\sum_j F_j-yd\sum_j jF_j=0 \ , \tag{3.29}$$

where F_i is the number of i-fold bonds and d is the common value of all bond lengths l_j determined by, say, the minimum in the pair potential. Referring to Eq. (3.21), we see that $\bar{q}$ after relaxation is

$$\bar{q}_{\text{ideal}}=2\pi/\cos^{-1}(\tfrac{1}{3}) \ . \tag{3.30}$$

Since the relaxation process preserves the bond topology, this is also the value of $\bar{q}$ for an ideal glass in flat space. Equation (3.30) agrees with the statistical honeycomb model of Coxeter, which assumes a network of identical Voronoi polygons with fractional numbers of faces.[7,9]

Figure 17 shows the values of $\bar{q}$ for the Frank-Kasper phases listed in Table IV as a function of the size of the unit cell. All values of q are remarkably close to the ideal-glass result with the accuracy increasing with unit-cell size. As the number of atoms in a unit cell gets larger, the system is better able to approximate the irra-

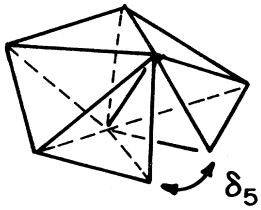

FIG. 16. Defect angle δ_5 for five perfect tetrahedra.

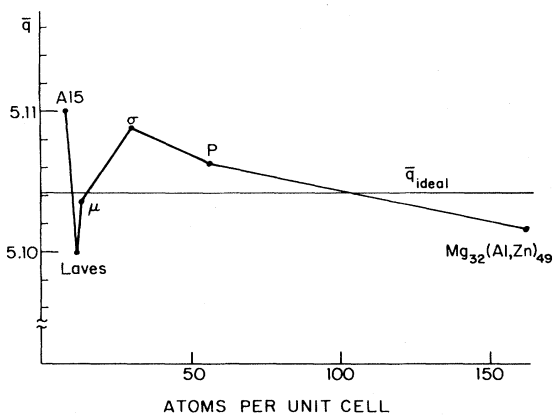

FIG. 17. Value of $\bar{q}$ for the Frank-Kasper phases as a function of the unit-cell size.

tional value (3.30). In this sense, we can regard an ideal glass as a Frank-Kasper phase with an infinitely large unit cell.

It is interesting to repeat the above argument for particles embedded in a space of constant positive Gaussian curvature κ^2. Prior to the relaxation, the integral on the right-hand side of Eq. (3.25) assumes the value

$$\tfrac{1}{2}{}^{(3)}R\,2\pi^2\kappa^{-3}=6\pi^2/\kappa\ , \tag{3.31}$$

where we have inserted the integral curvature of a 4D sphere,[43]

$${}^{(3)}R=6/\kappa^2\ , \tag{3.32}$$

and the surface area $2\pi^2\kappa^{-3}$ of a 4D sphere of radius κ^{-1}. Assuming that this value is unchanged by the relaxation process, we find that

$$\bar{q}_{ideal}=(2\pi/y)(1-3\pi/\kappa d N_b)\ , \tag{3.33}$$

where $N_b=\sum_i F_i$ is the total number of bonds in the system. Using Eq. (3.23), we see that N_b is related to the average coordination number $\bar{Z}$ and the total number of atoms N_a. We have

$$N_b=\tfrac{1}{2}N_a\bar{Z}\ . \tag{3.34}$$

Inserting (3.34) into (3.33) and using Eq. (3.19) to eliminate $\bar{Z}$ in favor of $\bar{q}_{ideal}$ leads to an equation which is easily solved for $\bar{q}_{ideal}$. One arrives in this way to the result Eq. (1.8a) quoted in the Introduction. The assumption that the integral curvature remains unchanged under relaxation is surely suspect in finite spaces like $S3$. We would expect deviations of order $1/\sqrt{N_a}$. This approximation is exact, however, for the ideal 120-particle tessellation since the tetrahedra formed by the near-neighbor bonds are already perfect. Inserting the curvature and volume per particle of the ideal tessellation into (1.8a), we find that

$$\bar{q}_{ideal}\approx 4.997\,717\ . \tag{3.35}$$

The small deviation from the exact result $\bar{q}_{ideal}=5$ for an icosahedral lattice is related to Regge's discretization procedure.

Equation (1.8a) can be applied to computer simulations of finite numbers of particles embedded in $S3$. This has already been done for particles in $S2$ as an alternative to periodic boundary conditions.[60] Such a simulation could be used to study the glass transition in three dimensions with the advantage that crystallization into lattices with cubic symmetry is automatically inhibited. For particle numbers such that

$$120<N_a\le\infty\ , \tag{3.36}$$

the curvature is incommensurate, and the ground state will be populated by an unpairable excess of icosahedral disclinations. An approximate estimate of the factor $\kappa v/d$ for N_a particles gives

$$\bar{q}_{ideal}(N_a)\doteq\frac{2\pi-3(6.46/N_a^{2/3})}{\cos^{-1}(\frac{1}{3})-\frac{1}{2}(6.46/N_a^{2/3})}\ . \tag{3.37}$$

For simulations of, say, 864 particles, which are well within the limitations of modern computers,[5] we find

$$\bar{q}_{ideal}(864)\approx 5.078\ , \tag{3.38}$$

which is rather close to the result (1.8b) for an infinite number of particles in flat space.

Figure 18 summarizes results for $\bar{q}$ and $\bar{Z}$ in a variety of different flat-space systems. Starting with a computer simulation of liquid argon,[61] these systems become progressively more ordered as $\bar{q}$ decreases. Note that the relaxed Ichikawa-Bennett model is further down on the curve than a perfect bcc crystal or an fcc crystal subjected to an infinitesimal shear stress ($\bar{q}=5\frac{1}{7}$ and $\bar{Z}=14$). The Frank-Kasper phases are clustered about the ideal-glass value. This progression can be viewed as a gradual pairing of plus and minus disclination lines until only $-72°$ disclinations are left in the "Frank-Kasper limit." We ex-

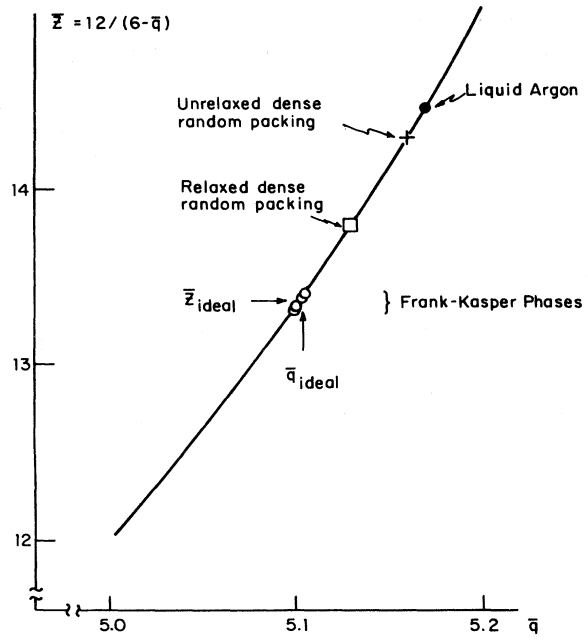

FIG. 18. Coordination number $\bar{Z}$ vs $\bar{q}$ for different kinds of particle configurations.

pect that increasing the number of 4-6 pairs will increase $\bar{Z}$ (and, hence $\bar{q}$) because there are many more coordination shells possible with multiple four- and sixfold bonds for $Z \geq 14$ than for $Z < 14$. If one excludes cooperative rearrangements of the lines, there need not be a sharp phase transition associated with this process. The ideal, "fully paired" structure is presumably quite similar locally to a Frank-Kasper phase. It need not be crystalline, however.

As the disclination network tries to become progressively more ordered, there are nontrivial kinetic constraints due to entanglement of defect lines in a non-Abelian medium.[20] When two non-Abelian defect lines attempt to cross, they cannot simply break and reform. Instead, they are joined by an umbilical defect $\gamma = \alpha\beta\alpha^{-1}\beta^{-1}$, where α and β are SU(2) matrices in $\pi_1(\mathrm{SO}(3)/Y)$ characterizing the crossing lines, and γ is the matrix describing the umbilical defect.[20] When two low-energy lines corresponding to rotations about different axes in an icosahedral medium cross, they always produce another low-energy line. If for example, $\alpha = U(\hat{n}_0, -72°)$ and $\beta = U(\hat{n}_5, -72°)$, straightforward matrix multiplication gives

$$\gamma = U(\hat{n}_0, -72°)U(\hat{n}_5, -72°)U^{-1}(\hat{n}_0, -72°)U^{-1}(\hat{n}_5, -72°)$$
$$= U(\hat{n}_2, -72°) . \quad (3.39)$$

The rotation axes $\hat{n}_0$, $\hat{n}_5$, and $\hat{n}_2$ are defined in Fig. 9.

Chemical short-range order, believed to play an important role in metallic glass formation, provides another important kinetic constraint. In metal-metalloid glasses, the minority metalloid constituents are believed to be surrounded by compact eight- and nine-particle coordination shells.[26] In amorphous Co-P, for example, every phosphorous atom is surrounded by a nine-atom cobalt coordination shell. These coordination shells are, in fact, just the three-and four-line nodes for $+72°$ disclinations shown in Fig. 14. Thus, seeding cobalt with phosphorous atoms amounts to seeding the material with nodes for disclination lines with the "wrong" sign—lines which would annihilate with their antidefect in the ideal-glass state. The chemistry of alloys which readily form Frank-Kasper phases presumably favors lines with the "right" sign.

It remains to be seen if a detailed and quantitative theory of glasses and supercooled liquids can be constructed using the ideas presented in this paper. It is nevertheless encouraging that, because the frustration scale κ_*^{-1} is so short, the defect density in a medium of icosahedra must be very high. In the Frank-Kasper phases, approximately 40—60 % of the atoms occupy defect sites. Specifying a disordered array of disclination lines essentially specifies the positions of all atoms up to small vibrations. Perhaps one can begin to understand why glasses appear disordered, and have, at the same time, a very low entropy.

ACKNOWLEDGMENTS

It is a pleasure to acknowledge helpful discussions with D. Eardley, P. Ginsparg, M. Rubinstein, J. Sethna, F. Spaepen, P. Steinhardt, and D. Turnbull. I am also indebted to M. Kléman, J. P. Gaspard, R. Mosseri, and J. F. Sadoc for stimulating conversations and for sending me their unpublished manuscripts prior to publication. J. L. Finney kindly supplied some of the information in Table III. This work was supported by the Alfred P. Sloan Foundation and by the National Science Foundation, through the Harvard University Materials Research Laboratory, and through Grant No. DMR-82-07431.

APPENDIX A: DEFECTS IN A CUBOCTAHEDRAL MEDIUM

In two dimensions there are an infinite number of regular polygons which give rise to an infinite number of commensurate particle packings as one varies κd in surfaces of positive and negative curvature. The situation is quite different in three dimensions, where there are only a finite number of Platonic solids. The most interesting case after the 13-particle icosahedron is a central atom surrounded by a six-particle cuboctahedral coordination shell. It is straightforward to show using the metric (3.4) that the eight tetrahedra which comprise a seven-particle cuboctahedron acquire equal edges when

$$\kappa d = \tilde{\kappa} d = \tfrac{1}{2}\pi \approx 1.57 . \quad (A1)$$

At this special curvature a 8-particle regular tessellation of $S3$ is possible,[8,9] such that each particle sits in a cuboctahedral environment. The required curvature is significantly larger than the icosahedral value (1.3). For curvatures such that

$$\kappa_* \ll \kappa \lesssim \tilde{\kappa} , \quad (A2)$$

or, equivalently, computer simulations of N_a particles in $S3$ such that

$$8 \lesssim N_a \ll 120 , \quad (A3)$$

the structure of the ground state can conveniently be described in terms of line disclination defects in a cuboctahedral medium.[62] The algebra of these defects is given by the homotopy group

$$\pi_1(\mathrm{S})(3)/\mathrm{O}) = \mathrm{O}' \quad (A4)$$

where O is the point group of the octahedron, and O′ is its lift into SU(2).

The same homotopy group describes line defects in a liquid crystal composed of molecules with a cubic symmetry.[20] Cubic bond orientational order, in liquids composed of isotropic particles, is also a possibility. As pointed out in Ref. 36, cubic crystalline solids disordered by a random array of dislocation loops should display a residual resistance to torsion not present in an isotropic liquid. The resulting anisotropic liquid is a cubic analog of the 2D hexatic phase. Line defects in such materials should form closed loops with combination laws given by (A4).

Figure 19 shows the three fourfold, four threefold, and six twofold symmetry axes of a cuboctahedron drawn in projection. The eight classes of O′ are, in the notation of Sec. II C,

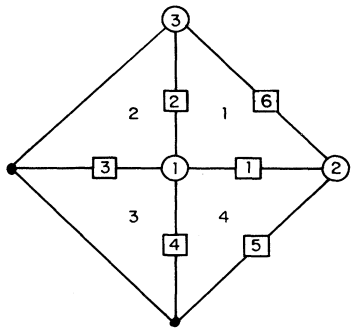

FIG. 19. Symmetry axes of a cuboctahedron drawn in projection about the fourfold axis labeled "1" at the origin. Vertex opposite "1" is not shown.

$$\mathscr{C}_0=\{1\}\ ,\quad \mathscr{C}_0=\{-1\}\ ,$$

$$\mathscr{C}_4=\{U(\hat{n}_i,90°),U(\hat{n}_i,-90°)\ ,i=1,\ldots,3\}\ ,$$

$$\overline{\mathscr{C}}_4=\{U(\hat{n}_i,270°),U(\hat{n}_i,-270°)\ ,i=1,\ldots,3\}\ ,$$

$$\mathscr{C}_4^2=\{U(\hat{n}_i,180°)\ ,U(\hat{n}_i,-180°)\ ,i=1,\ldots,3\}\ ,$$

$$\mathscr{C}_3=\{U(\hat{m}_i,120°)\ ,U(\hat{m}_i,-120°)\ ,i=1,\ldots,4\}\ ,$$

$$\overline{\mathscr{C}}_3=\{U(\hat{m}_i,240°)\ ,U(\hat{m}_i,-240°)\ ,i=1,\ldots,4\}\ ,$$

$$\mathscr{C}_2=\{U(\hat{l}_i,180°)\ ,U(\hat{l}_i,-180°)\ ,i=1,\ldots,6\}\ .$$

The class multiplication table is displayed in Table V. The class $\mathscr{C}_4$ (consisting of $\pm 90°$ disclination lines) is the analog of the class of low-energy $\pm 72°$ disclination lines in an icosahedral medium. According to Table V,

$$\mathscr{C}_4\times\mathscr{C}_4=6\mathscr{C}_0+\mathscr{C}_4^2+3\mathscr{C}_3\ , \tag{A5}$$

so two low-energy lines cannot combine to form a third one. Unlike the icosahedral case, three-line nodes in a network of low-energy lines are impossible. As in the icosahedral case, more exotic defects can be made appropriately chosen bundles of low-energy lines.

Just as for icosahedral disclination lines, it is difficult for two low-energy cuboctahedral lines corresponding to rotations about different symmetry axes to cross. The umbilical defect which results (see Sec. II C) is a 120° rotation about a threefold symmetry axis. If, for example, $\alpha=U(\hat{n}_1,-90°)$ and $\beta=U(\hat{n}_2,-90°)$, the resulting umbilical defect is

$$\gamma=\alpha\beta\alpha^{-1}\beta^{-1}=U(\hat{m}_2,-120°)\ . \tag{A6}$$

APPENDIX B: COMPARISON WITH THE BLUE PHASES OF CHOLESTERIC LIQUID CRYSTALS

The free energy of a cholesteric nematic liquid crystal is, in the one-Frank-constant approximation,[37,38]

$$F=\tfrac{1}{2}K\int(\partial_i n^j-q_0\epsilon_{ijk}n^k)^2\ , \tag{B1}$$

where $\vec{n}$ is a unit vector directed along a local uniaxial symmetry axis. This free energy is clearly a specialization of Eq. (3.12) to the case of a single unit vector, with

$$M^j_{ik}=q_0\epsilon_{ijk}\ . \tag{B2}$$

Sethna has, in fact, interpreted the operator acting on $\vec{n}$ in Eq. (B1) as the covariant derivative appropriate to a curved surface with both curvature and torsion.[63] Meiboom *et al.*[37,38] have argued that the blue phases of cholesterics are a regular array of disclination lines. Networks of coreless $+1$ disclinations are threaded by a conjugate defect network of ordinary $-\frac{1}{2}$ nematic disclination lines.[38] Kléman[11] has suggested that a similar conjugated network of disclination lines should appear in glasses.

TABLE V. Class multiplication table for the group O′.

$\mathscr{C}_0$	$\overline{\mathscr{C}}_0$	$\mathscr{C}_4$	$\overline{\mathscr{C}}_4$	$\mathscr{C}_4^2$	$\mathscr{C}_3$	$\overline{\mathscr{C}}_3$	$\mathscr{C}_2$
$\overline{\mathscr{C}}_0$	$\mathscr{C}_0$	$\overline{\mathscr{C}}_4$	$\mathscr{C}_4$	$\mathscr{C}_4^2$	$\overline{\mathscr{C}}_3$	$\mathscr{C}_3$	$\mathscr{C}_2$
$\mathscr{C}_4$		$6\mathscr{C}_0+\mathscr{C}_4^2$ $+3\mathscr{C}_3$	$6\overline{\mathscr{C}}_0+\mathscr{C}_4^2$ $+3\overline{\mathscr{C}}_3$	$\mathscr{C}_4+\overline{\mathscr{C}}_4$ $+2\mathscr{C}_2$	$4\mathscr{C}_4+2\mathscr{C}_2$	$4\overline{\mathscr{C}}_4+2\mathscr{C}_2$	$2\mathscr{C}_4^2+3\mathscr{C}_3$ $+3\overline{\mathscr{C}}_3+\mathscr{C}_2$
$\overline{\mathscr{C}}_4$			$6\mathscr{C}_0+\mathscr{C}_4^2$ $+3\mathscr{C}_3$	$\mathscr{C}_4+\overline{\mathscr{C}}_4$ $+2\mathscr{C}_2$	$4\overline{\mathscr{C}}_4+2\mathscr{C}_2$	$4\mathscr{C}_4+2\mathscr{C}_2$	$2\mathscr{C}_4^2+3\mathscr{C}_3$ $+3\overline{\mathscr{C}}_3+\mathscr{C}_2$
$\mathscr{C}_4^2$				$6\mathscr{C}_0+6\overline{\mathscr{C}}_0$ $+2\mathscr{C}_4^2+\mathscr{C}_2$	$3\mathscr{C}_3+3\overline{\mathscr{C}}_3$	$3\mathscr{C}_3+3\overline{\mathscr{C}}_3$	$4\mathscr{C}_4+4\overline{\mathscr{C}}_4$ $+2\mathscr{C}_2$
$\mathscr{C}_3$					$8\mathscr{C}_0+2\mathscr{C}_4^2$ $+3\mathscr{C}_3+\overline{\mathscr{C}}_3$ $+\mathscr{C}_2$	$8\overline{\mathscr{C}}_0+2\mathscr{C}_4^2$ $+\mathscr{C}_3+3\overline{\mathscr{C}}_3$ $+\mathscr{C}_2$	$4\mathscr{C}_4+4\overline{\mathscr{C}}_4$ $+4\mathscr{C}_2$
$\overline{\mathscr{C}}_3$						$8\mathscr{C}_0+2\mathscr{C}_4^2$ $+3\mathscr{C}_3+\overline{\mathscr{C}}_3+\mathscr{C}_2$	$4\mathscr{C}_4+\overline{\mathscr{C}}_4$ $+4\mathscr{C}_2$
$\mathscr{C}_2$							$12\mathscr{C}_0+12\overline{\mathscr{C}}_0$ $+2\mathscr{C}_4^2+6\mathscr{C}_3$ $+6\overline{\mathscr{C}}_3+\mathscr{C}_2$

Although this is apparently not what occurs in the Frank-Kasper phases, there *is* something reminiscent of twisted cholesteric order in the 1D three-stranded "Bernal spiral" particle packing shown in Fig. 20.[5] Bernal associated these arrangements of perfect tetrahedra with "colineations" of particles he found throughout his dense-random-packing models.[25] A recursion relation which generates the nth particle of the spiral given the preceding three-particle positions is

$$\vec{x}_n=\vec{x}_{n-1}+\vec{x}_{n-2}+\vec{x}_{n-3}\pm\frac{2\sqrt{3}}{3d}(\vec{x}_{n-3}-\vec{x}_{n-2})\times(\vec{x}_{n-2}-\vec{x}_{n-1})\,, \qquad \text{(B3)}$$

where the plus and minus signs give right- and left-handed spirals, respectively, and d is the particle spacing. Coxeter has shown that this spiral has an irrational pitch.[9] Following the spiral along one of its strands for 10 links, one returns to the original configuration shifted by about $6\frac{2}{3}$ deg about the spiral axis. Remarkably, this spiral *fits perfectly* into the 120-particle commensurate tessellation of $S3$.[8,9]

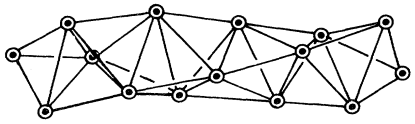

FIG. 20. Three-stranded spiral formed by a 1D array of perfect tetrahedra.

True cholesteric order, however, would require an excess of, say, right-handed spirals over left-handed ones. It is hard to see an energetic reason why structureless particles should exhibit a chiral broken symmetry. It can, in fact, be shown that the ideal 120-particle tessellation of $S3$ is a "racemic" mixture of equal numbers of left- and right-handed spirals. By allowing cholesteric molecules to follow either the left- or right-hand set of spirals, one obtains a perfect blue-phase liquid-crystal texture in $S3$.[64]

[1]P. Chaudhari and D. Turnbull, Science A 199, 11 (1978).

[2]F. C. Frank, Proc. R. Soc. London Ser. A 215, 43 (1952).

[3]The energy of a 13-atom icosahedron is lower than the corresponding fcc or hcp clusters by 3.58ϵ for a Lennard-Jones potential where ϵ is the Lennard-Jones energy parameter. The difference arises because 42 bonds in an icosahedral cluster are approximately at the minimum of the pair potentials, as opposed to 36 bonds in fcc or hcp 13-atom clusters.

[4]D. Turnbull, J. Chem. Phys. 20, 411 (1952).

[5]P. J. Steinhardt, D. R. Nelson, and M. Ronchetti, Phys. Rev. Lett. 47, 1297 (1981); Phys. Rev. B 28, 784 (1983).

[6]M. R. Hoare, Ann. N. Y. Acad. Sci. 279, 186 (1976).

[7]H. S. M. Coxeter, Ill. J. Math. 2, 746 (1958).

[8]H. S. M. Coxeter, *Regular Polytopes* (Dover, New York, 1973).

[9]H. S. M. Coxeter, *Introduction to Geometry* (Wiley, New York, 1969).

[10]M. Kléman and J. F. Sadoc, J. Phys. (Paris) Lett. 40, L569 (1979).

[11]M. Kléman, J. de Phys. 43, 1389 (1982); in *Continuum Models of Discrete Systems,* edited by O. Brulin and R. K. T. Hsieh (North-Holland, Amsterdam, 1981); J. Phys. (Paris) Lett. 44, L295 (1983).

[12]J. F. Sadoc, J. Phys. (Paris) Colloq. 41, C8-326 (1980).

[13]J. F. Sadoc and R. Mosseri, Philos. Mag. B 45, 467 (1982).

[14]F. C. Frank and J. S. Kasper, Acta Crystallogr. 11, 184 (1958); 12, 483 (1959).

[15]D. R. Nelson, Phys. Rev. Lett. 50, 982 (1983).

[16]B. I. Halperin and D. R. Nelson, Phys. Rev. Lett. 41, 121; 41, 519(E) (1978); D. R. Nelson and B. I. Halperin, Phys. Rev. B 19, 2457 (1979).

[17]A. P. Young, Phys. Rev. B 19, 1855 (1979).

[18]J. M. Kosterlitz and D. J. Thouless, J. Phys. C 6, 1181 (1973).

[19]D. R. Nelson, in *Topological Disorder in Condensed Matter,* edited by F. Yonezawa and T. Ninomiya (Springer, Berlin, 1983).

[20]N. D. Mermin, Rev. Mod. Phys. 51, 591 (1979).

[21]A. M. Kosevich, in *Dislocations in Solids,* edited by F. R. N. Nabarro (North-Holland, Amsterdam, 1979), Vol 1.

[22]See, e.g., R. Collins, in *Phase Transitions and Critical Phenomena,* edited by C. Domb and M. S. Green (Academic, New York, 1972), Vol. II. As explained in this reference, the Dirichlet and Voronoi constructions generalize the idea of a Wigner-Seitz cell to 2D and 3D disordered particle arrays. With this definition, bcc and fcc lattices have, respectively, coordination numbers 14 and 12. As discussed in Sec. III, the coordination number of an fcc lattice becomes 14 upon application of an infinitesimal shear distortion.

[23]J. P. McTague, D. Frankel, and M. Allen, in *Ordering in Two Dimensions,* edited by S. Sinha (North-Holland, Amsterdam, 1980).

[24]D. R. Nelson, Phys. Rev. B 26, 269 (1982).

[25]J. D. Bernal, Proc. R. Soc. London Ser. A 280, 299 (1964).

[26]See, e.g., F. Spaepen, in *Rapidly Quenched Metals,* edited by B. Cantor (The Metals Society, London, 1979).

[27]J. P. Gaspard, R. Mosseri, and J. F. Sadoc, in Proceedings of the Conference on Structure of Noncrystalline Materials, Cambridge, England, July, 1982 (in press).

[28]The importance of the Frank-Kasper phases in understanding disclination models of glass has also been pointed out by J. F. Sadoc, Orsay report (unpublished).

[29]N. Rivier, Philos. Mag. A 40, 859 (1979); in Trans. Metals Soc. AIME (Fall Meeting, 1982), edited by V. Vitek (in press).

[30]P. W. Anderson, in *Ill-Condensed matter,* edited by R. Balien, R. Maynard, and G. Toulouse (North-Holland, Amsterdam, 1979).

[31]T. Ninomiya, in *Topological Disorder in Condensed Matter,* edited by F. Yonezawa and T. Ninomiya (Springer, Berlin, 1983). In two dimensions, the analogous approach is to regard disordered materials as mixtures of triangles and squares. See R. Collins, Proc. Phys. Soc. London 83, 553 (1964).

[32]G. Toulouse, Commun. Phys. 2, 115 (1977).

[33]J. Villain, J. Phys. C 10, 1717 (1977); C 10, 4793 (1977); C 11, 745 (1978); E. Fradkin, B. A. Huberman, and S. H. Shenker, Phys. Rev. B 18, 4789 (1978).

[34]S. Teitel and C. Jayaprakash, Phys. Rev. B 27, 598 (1983).

[35]Although there are no physical examples of materials on surfaces of *constant* negative curvature, the *mean* Gaussian curvature on a porous surface like Vycor glass is negative.

[36]D. R. Nelson and J. Toner, Phys. Rev. B 24, 363 (1981).

[37]S. Meiboom, J. P. Sethna, P. W. Anderson, W. F. Brinkman, Phys. Rev. Lett. 46, 1216 (1981).

[38]S. Meiboom, M. Sammon, and W. F. Brinkman, Phys. Rev. A 27, 438 (1982).

[39]W. F. Brinkman, D. S. Fisher, and D. E. Moncton, Science 217, 693 (1982).

[40]For recent experimental evidence supporting continuous melting into a hexatic phase for xenon films on graphite, see T. F. Rosenbaum, S. E. Nagler, P. M. Horn, and R. Clarke, Phys. Rev. Lett. 50, 1796 (1983). For experimental evidence of a two-layer, hexatic liquid-crystal film, see J. Budai, S. C. Davey, D. E. Moncton, and R. Pindak, Bull. Am. Phys. Soc. 28, 332 (1983).

[41]These figures are taken from a computer simulation of particles interacting with a repulsive $1/r$ potential by R. Morf.

[42]L. D. Landau and E. M. Lifshitz, *The Classical Theory of Fields* (Pergamon, New York, 1971), Chaps. 10—12.

[43]C. W, Misner, K. S. Thorne, and J. A. Wheeler, *Gravitation* (W. H. Freeman, San Francisco, 1971).

[44]M. Tinkham, *Introduction to Superconductivity* (McGraw-Hill, New York, 1975).

[45]I. M. Singer, Physics Today 35(3), 41 (1982); see also W. Drechsler and M. E. Mayer, *Fiber Bundle Techniques in Gauge Theories,* Vol. 67 of *Lecture Notes in Physics* (Springer, Berlin, 1977).

[46]D. S. Fisher, Phys. Rev. B 22, 1190 (1980), and references therein. There is also a close analogy with rotating superfluid He^4; see W. F. Vinen, in *Superconductivity,* edited by R. D. Parks (Dekker, New York, 1969), Vol. 2.

[47]C. H. Bennett, J. Appl. Phys. 43, 2727 (1972).

[48]This figure was prepared by M. Rubinstein; see M. Rubinstein and D. R. Nelson (unpublished).

[49]H. Suzuki, in *Topological Disorder in Condensed Matter,* Ref. 31.

[50]A. Zippelius, B. I. Halperin, and D. R. Nelson, Phys. Rev. B 22, 2514 (1980).

[51]G. S. Grest, S. R. Nagel, and A. Rahman, Phys. Rev. Lett. 49, 1271 (1982).

[52]J.-F. Sadoc, J. Dixmier, and A. Guinier, J. Non-Cryst. Solids 12, 46 (1973).

[53]A useful source of geometrical information on the icosahedron is *CRC Standard Mathematical Tables,* edited by S. M. Selby (The Chemical Rubber Co., Cleveland, 1970), pp. 15 and 16.

[54]We have used the standard result that $\Gamma^k_{ij}=g^{kl}\Gamma_{ij,l}$ where

$$\Gamma_{ij,l}=\tfrac{1}{2}(\partial_i g_{jl}+\partial_j g_{il}-\partial_l g_{ij})$$

(see Refs. 42 and 43).

[55]R. Yamamoto, H. Shibuta, T. Mihara, K. Haga, and M. Doyama, in *Proceedings of the International Conference on Rapidly Quenched Metals,* edited by T. Masumoto and K. Suzuki (Japan Institute of Metals, Sendai, 1982), Vol. 1.

[56]T. Ichikawa, Phys. Status Solidi 19, 707 (1973).

[57]J. L. Finney, Proc. R. Soc. London Ser. A 319, 479 (1970).

[58]J. Andrew Barker, J. L. Finney, and M. R. Hoare, Nature 257, 120 (1975).

[59]Our value $\bar{Z}=13.38$ for the μ phase of Fe_7W_6 is different from the result $\bar{Z}=13.2$ quoted in Ref. 14.

[60]J. P. Hansen, D. Levesque, and J. J. Weis, Phys. Rev. Lett. 43, 979 (1983). For packings in $S3$, see A. L. Mackay, J. Phys. A 13, 3373 (1980).

[61]A. Rahman, J. Chem. Phys. 45, 2585 (1966).

[62]For curvatures $\kappa \gtrsim \kappa_*$, the ground state is better described in terms of an excess of $+72°$ icosahedral disclinations.

[63]J. Sethna (unpublished).

[64]I am grateful for discussions with D. Eardley on this point. See also J. P. Sethna, D. C. Wright, and N. D. Mermin, Phys. Rev. Lett. 51, 467 (1983). For a closely related calculation in SO(3), see exercise 10.17 in Ref. 43.